

# The function of CozE proteins is linked to lipoteichoic acid biosynthesis in *Staphylococcus aureus*

Maria Disen Barbuti,<sup>1</sup> Elisabeth Lambert,<sup>2</sup> Ine Storaker Myrbråten,<sup>1</sup> Adrien Ducret,<sup>3</sup> Gro Anita Stamsås,<sup>1</sup> Linus Wilhelm,<sup>3</sup> Xue Liu,<sup>4,5</sup> Zhian Salehian,<sup>1</sup> Jan-Willem Veening,<sup>5</sup> Daniel Straume,<sup>1</sup> Christophe Grangeasse,<sup>3</sup> Camilo Perez,<sup>2,6</sup> Morten Kjos<sup>1</sup>

**AUTHOR AFFILIATIONS** See affiliation list on p. 20.

**ABSTRACT** Coordinated membrane and cell wall synthesis is vital for maintaining cell integrity and facilitating cell division in bacteria. However, the molecular mechanisms that underpin such coordination are poorly understood. Here we uncover the pivotal roles of the staphylococcal proteins CozEa and CozEb, members of a conserved family of membrane proteins previously implicated in bacterial cell division, in the biosynthesis of lipoteichoic acids (LTA) and maintenance of membrane homeostasis in *Staphylococcus aureus*. We establish that there is a synthetic lethal relationship between CozE and UgtP, the enzyme synthesizing the LTA glycolipid anchor Glc<sub>2</sub>DAG. By contrast, in cells lacking LtaA, the flippase of Glc<sub>2</sub>DAG, the essentiality of CozE proteins was alleviated, suggesting that the function of CozE proteins is linked to the synthesis and flipping of the glycolipid anchor. CozE proteins were indeed found to modulate the flipping activity of LtaA *in vitro*. Furthermore, CozEb was shown to control LTA polymer length and stability. Together, these findings establish CozE proteins as novel players in membrane homeostasis and LTA biosynthesis in *S. aureus*.

**IMPORTANCE** Lipoteichoic acids are major constituents of the cell wall of Gram-positive bacteria. These anionic polymers are important virulence factors and modulators of antibiotic susceptibility in the important pathogen *Staphylococcus aureus*. They are also critical for maintaining cell integrity and facilitating proper cell division. In this work, we discover that a family of membrane proteins named CozE is involved in the biosynthesis of lipoteichoic acids (LTAs) in *S. aureus*. CozE proteins have previously been shown to affect bacterial cell division, but we here show that these proteins affect LTA length and stability, as well as the flipping of glycolipids between membrane leaflets. This new mechanism of LTA control may thus have implications for the virulence and antibiotic susceptibility of *S. aureus*.

**KEYWORDS** teichoic acids, cell division, membrane homeostasis, membrane proteins

*Staphylococcus aureus* is a Gram-positive, opportunistic pathogen that is responsible for a wide range of infectious diseases in humans and animals, including skin and soft tissue infections, bloodstream infections, and infections associated with medical implant devices. This is made possible by the plethora of virulence factors produced by *S. aureus*. Among the major factors contributing to staphylococcal colonization, infection, and immune evasion are the anionic teichoic acid (TA) polymers (1, 2). Together with peptidoglycan, TAs are the main constituents of the staphylococcal cell wall. Interestingly, TAs influence the susceptibility of *S. aureus* to antibiotics (1, 3), making the TA biosynthetic pathways attractive as potential anti-virulence and antibiotic targets.

Staphylococcal TAs are mainly composed of repeating units of ribitol phosphate (RboP) or glycerol phosphate (GroP) that are either covalently linked to peptidoglycan (wall teichoic acids, WTAs) or anchored to the cytoplasmic membrane (lipoteichoic

**Editor** Lotte Søgaard-Andersen, Max-Planck-Institut für terrestrische Mikrobiologie, Marburg, Germany

Address correspondence to Morten Kjos, morten.kjos@nmbu.no.

The authors declare no conflict of interest.

See the funding table on p. 21.

**Received** 15 April 2024

**Accepted** 21 April 2024

**Published** 17 May 2024

Copyright © 2024 Barbuti et al. This is an open-access article distributed under the terms of the [Creative Commons Attribution 4.0 International license](https://creativecommons.org/licenses/by/4.0/).

acids, LTAs). Although LTA is more important than WTA for cell viability, it is possible to create deletion mutants of genes involved in either pathway. However, it is not possible to delete both pathways simultaneously (4, 5). Staphylococcal LTAs consist of poly-GroP chains that are associated with the cytoplasmic membrane through the glycolipid anchor diglucosyl-diacylglycerol (Glc<sub>2</sub>DAG) (Fig. 3A). Glc<sub>2</sub>DAG is synthesized in the cytoplasm by the glycosyltransferase UgtP (also called YpfP), which transfers two glucose moieties from uridine diphosphate glucose (UDP-Glc) to DAG (6). Glc<sub>2</sub>DAG is then translocated to the outer membrane leaflet by the multi-membrane spanning protein LtaA (7, 8). Lastly, the LTA synthase, LtaS, polymerizes the poly-GroP backbone chain by transferring GroP units, derived from the head group of phosphatidylglycerol (PG), to the Glc<sub>2</sub>DAG, on the outside surface of the membrane (9), leaving extracellular DAG as a by-product. LTA polymers are often further modified by D-alanylation, carried out by the DltABCD system, and/or glycosylation, which modulates their properties and functions (10, 11).

In *S. aureus*, deletion of the gene encoding the LTA synthase (*ltaS*), resulting in cells completely devoid of LTA, is only possible in the presence of suppressor mutations (12, 13). Cells with deletion of the genes required for synthesis and flipping of the glycolipid anchor ( $\Delta$ *ugtP* and  $\Delta$ *ltaA*, respectively) are however still viable (6, 14). In  $\Delta$ *ugtP* cells, which completely lack the Glc<sub>2</sub>DAG anchor, LtaS initiates LTA synthesis directly on PG (6, 15).  $\Delta$ *ltaA* mutants have been demonstrated to produce a mixture of LTAs linked to both PG and Glc<sub>2</sub>DAG (7); hence, there must exist an unidentified mechanism that can translocate Glc<sub>2</sub>DAG, produced by UgtP, to the outer membrane leaflet in the absence of LtaA. In both  $\Delta$ *ugtP* and  $\Delta$ *ltaA* cells, LTA length control is lost, resulting in cells that produce PG-linked LTA polymers which are abnormally long and less stably anchored in the membrane (7, 16, 17).

Importantly, several studies suggest a tight link between LTA synthesis and cell division in *S. aureus*. Deletion of genes in the LTA biosynthetic pathway results in enlarged cells with severe division and morphological defects, suggested to be caused by changes in LTA length and abundance (6, 14, 15, 18). Furthermore, UgtP, LtaA, and LtaS have all been shown to interact with each other and with multiple cell division and cell wall synthesis proteins (e.g., EzrA, FtsA, FtsW, and PBP1-PBP4) (19). LtaS has also been demonstrated to accumulate mainly at the septum in *S. aureus*, indicating that LTA synthesis predominantly occurs at the division site (19). Together, this suggests that LTA biosynthesis is tightly coordinated with peptidoglycan synthesis and other processes during the staphylococcal cell cycle (20).

CozE (c<sub>o</sub>ordinator of z<sub>o</sub>nal e<sub>l</sub>ongation) belongs to a family of multi-transmembrane proteins that are broadly distributed across the bacterial kingdom (21). CozE (also referred to as CozEa) was first studied in *Streptococcus pneumoniae*, where it was shown to direct localization of peptidoglycan synthesis, possibly via interactions with the bifunctional class A PBP1a and the MreCD complex involved in cell morphogenesis (21–23). Later studies have also indicated functional interactions with additional morphogenesis factors, such as RodZ (24). A CozE paralog in *S. pneumoniae*, named CozEb, has also been found to be part of the same complex as CozE (24, 25), and there seems to be a complex interplay between the two paralogs (24, 25); individual deletions of *cozE* or *cozEb* in *S. pneumoniae* generated different phenotypes with regard to cell shape and growth inhibition, and while CozEb was not required for correct localization of PBP1a, overexpression of this protein could compensate for deletion of *cozE*, suppressing both growth and morphology defects.

In *S. aureus*, the two CozE-paralogs, CozEa and CozEb, have been studied in the strain SH1000, where they were found to be important for proper cell division (26). While neither *cozEa* nor *cozEb* was essential when deleted individually, a synthetic lethal phenotype was observed; a double deletion strain could not be obtained and knock-down of *cozEa* in a  $\Delta$ *cozEb* background (or vice versa) resulted in significantly reduced growth, aberrant septal placement, distorted cell morphologies, frequent cell lysis, and a non-homogeneous nucleoid staining (26). CozEa and CozEb were found to interact with

and modulate the localization of the cell division regulator EzrA, suggesting that this interaction may be important for the coordination of cell division in this bacterium (26).

In this work, we demonstrate that there is a functional link between the biosynthesis of LTA and CozE proteins in *S. aureus*. We show that the two CozE proteins have unique functionalities, as CozEb, but not CozEa, modulates the length and stability of LTAs and the flipping activity of LtaA *in vitro*. The results presented here give insights into hitherto unknown functions of the broadly distributed CozE proteins.

## RESULTS

### CozEa and CozEb affect cell division across different *Staphylococcus aureus* strains

In previous work, we showed that *cozEa* and *cozEb* in *S. aureus* SH1000 were synthetic lethal and possessed overlapping effects on growth and cell morphology (26). To investigate the functional conservation of *cozEa* and *cozEb* across different *S. aureus* strains and to characterize the phenotypes in more detail,  $\Delta\text{cozEa}::\text{spc}$  and  $\Delta\text{cozEb}::\text{spc}$  mutants were constructed in the methicillin-sensitive *S. aureus* (MSSA) strain NCTC8325-4, while the *cozEa::Tn* and *cozEb::Tn* mutants in the community-associated methicillin-resistant *S. aureus* (CA-MRSA) USA300 strain JE2 were obtained from the Nebraska collection (27). Neither of the single deletions resulted in any growth defects under the conditions tested, and no obvious morphological defects were found by microscopy analysis (Fig. 1A and B; Fig. S1A, S2A and B). The cell sizes were not severely altered, although the JE2  $\Delta\text{cozEa}$  cells, as well as both NCTC8325-4 *cozE* mutants, on average were slightly smaller than their wild-types (Fig. 1B through D; Fig. S2B through D). Likewise, cell cycle phase distribution analysis (performed on cells with fluorescent vancomycin-labeled cell wall; Fig. 1B; Fig. S2B) (28) did not reveal differences between mutant and wild-type cells (Fig. 1E and F; Fig. S2E). Thus, the *cozEa* and *cozEb* mutants in JE2 and NCTC8325-4 were similar to their respective wild-types, which is consistent with the results from *S. aureus* SH1000 (26).

Similar to what was reported previously (26), we were unable to obtain a double  $\Delta\text{cozEa}\Delta\text{cozEb}$  mutant in NCTC8325-4 by allelic replacement using the pMAD-vector (29). We therefore used an established two-plasmid CRISPR interference (CRISPRi) system for the knockdown of gene expression (26, 30). In this system, dCas9 is expressed from an IPTG-inducible promoter on one plasmid, and the gene-specific sgRNA is constitutively expressed from the other. Indeed, simultaneous knockdown of *cozEa* and *cozEb* in wild-type backgrounds, knockdown of *cozEa* in the  $\Delta\text{cozEb}$  backgrounds [ $\Delta\text{cozEb}$ , CRISPRi(*cozEa*)] or vice versa caused a clear growth reduction in both JE2 and NCTC8325-4 (Fig. 1A; Fig. S1B and S2A). These cells also exhibited perturbed cell sizes, shapes, and septa compared to the wild-type cells and single deletions (Fig. 1B through D and G; Fig. S2B through D). By categorizing the cells into three cell cycle phases based on fluorescent vancomycin (VanFL) labeling (Fig. 1E), we observed over-representation of phase 1 cells (cells before initiating septum synthesis) and under-representation of phase 2 (cells with incomplete septa) and phase 3 cells (cell with complete septa) (Fig. 1F; Fig. S2E), showing that coordination of cell division is disturbed in cells lacking both CozE proteins. More specifically, this indicates that initiation of septum synthesis is inhibited in these cells.

### Cells lacking both CozE proteins have mis-localized cell wall synthesis

Localization of peptidoglycan synthesis was further investigated by labeling cells with the fluorescent D-amino acid 7-hydroxycoumarincarboxylamino-D-alanine (HADA) (31). Since HADA is incorporated into newly synthesized peptidoglycan via transpeptidation during the labeling period, it is possible to distinguish sites of active growth. In this study, the cells were incubated with HADA for 2 minutes at 37°C. Single deletions of *cozEa* or *cozEb* did not have an impact on the localization of nascent peptidoglycan in JE2 nor NCTC8325-4, it was located properly in the septal region (Fig. 2). However, when

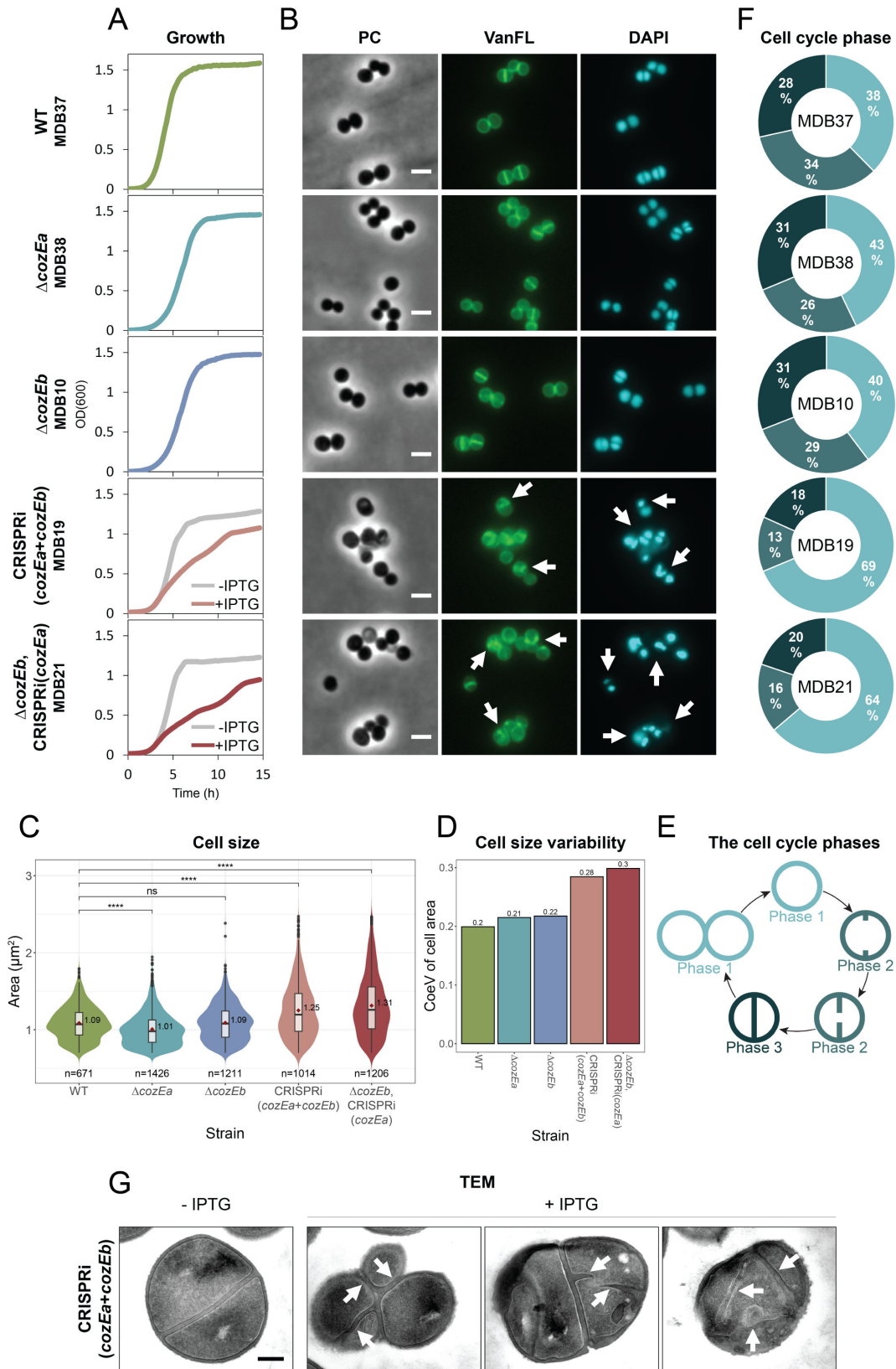


**FIG 1** Morphological and cell cycle analysis of single and double *cozE* mutants in *S. aureus* JE2. (A) Growth curves of JE2 wild-type (MDB37),  $\Delta$ cozEa::Tn (MDB38), and  $\Delta$ cozEb::Tn (MDB10), as well as of a CRISPRi double knockdown strain [CRISPRi(*cozEa* + *cozEb*), MDB19] and a combined knockout/knockdown (Continued on next page)

**FIG 1** (Continued)

strain [ $\Delta\text{cozEb}$  + CRISPRi(*cozEa*), MDB21] in BHI medium at 37°C. The graphs represent averages from triplicate measurements. The CRISPRi strains were grown with and without IPTG, as indicated. Note that all CRISPRi strains, in this study, started growing rapidly after approximately 10 hours. This phenomenon is most likely caused by reduced functionality of the CRISPRi system in this experimental setup beyond the 10-hour mark. (B) Micrographs of the same strains as in panel A showing phase contrast (PC) and fluorescence microscopy of cells stained with the cell wall label VanFL and the nucleoid label DAPI. CRISPRi strains were grown in a medium with IPTG to induce the CRISPRi system. White arrows point to cells with perturbed septum formation and abnormal nucleoid staining. The scale bars are 2  $\mu\text{m}$ . (C) Violin plots of the cell areas (in  $\mu\text{m}^2$ ) of JE2 wild-type ( $1.09 \pm 0.22 \mu\text{m}^2$ ),  $\Delta\text{cozEa}::\text{Tn}$  ( $1.01 \pm 0.22 \mu\text{m}^2$ ),  $\Delta\text{cozEb}::\text{Tn}$  ( $1.09 \pm 0.24 \mu\text{m}^2$ ), MDB19 ( $1.25 \pm 0.36 \mu\text{m}^2$ ), and MDB21 ( $1.31 \pm 0.39 \mu\text{m}^2$ ), determined using MicrobeJ. Significant differences between the strains are indicated with asterisks (\* indicates a *P*-value of <0.05, \*\* indicates a *P*-value of <0.01, and \*\*\* indicates a *P*-value of <0.001, derived from the Mann-Whitney test). The number of cells analyzed for each strain is indicated in the figure. (D) Coefficient of variance (CoeV) of cell size for each strain based on the data provided in (C), showing the relative dispersion of cell area for each strain around their perspective means (CoeV = standard deviation of cell area/mean cell area). (E) Schematic outline of the different cell cycle phases used to classify the cells in (F). Cells in phase 1 are non-dividing cells without visible septa, cells in phase 2 are actively dividing cells with incomplete septa, and cells in phase 3 are dividing cells with fully formed septa. (F) Frequency of cells in each of the three cell cycle phases for JE2 wild-type,  $\Delta\text{cozEa}::\text{Tn}$ ,  $\Delta\text{cozEb}::\text{Tn}$ , MDB19, and MDB21. The distributions were obtained by manually counting the different cell cycle phases of 100–150 randomly selected VanFL-stained cells from each strain. (G) TEM micrographs of uninduced and induced CRISPRi(*cozEa* + *cozEb*) (MDB19) cells. White arrows point to cells with aberrant septum formation. The scale bar is 200 nm.

both CozE proteins were absent, the HADA signals were highly heterogeneous with respect to signal intensity, and frequently appeared as clustered aggregates instead of being localized at the septum (Fig. 2A and B). Both the JE2 and NCTC8325-4 double *cozE* mutants displayed a high frequency of abnormal HADA labeling (Fig. 2C and D). Similar to what we observed above (Fig. 1; Fig. S1 and S2), the phenotypic defects of the deletion-depletion strain [ $\Delta\text{cozEa}$ , CRISPRi(*cozEb*)], Fig. 2B and D] were more severe than that of the double depletion strain [CRISPRi(*cozEa* + *cozEb*)], Fig. 2A and C]. These observations show that peptidoglycan synthesis in *S. aureus* is mis-localized when both CozE proteins are absent.

### The *cozE* genes have a synthetic link to genes involved in LTA synthesis

Mutants lacking both CozE proteins exhibited distinctive phenotypic traits, such as morphological abnormalities and impaired control of septum formation (Fig. 1 and 2; Fig. S2) (25). This resembles the phenotypes of *S. aureus* mutants with defects in LTA biosynthesis ( $\Delta\text{ItaS}$ ,  $\Delta\text{ItaA}$ , or  $\Delta\text{ugtP}$ ) (4, 6, 7, 9, 14) (Fig. 3A). In this context, it is also interesting to note that in a study by Corrigan et al. (12), re-sequencing of *ItaS* deletion mutants resulted in potential suppressor mutations in *cozEb* (SAOUHSC\_01358). This prompted us to investigate a potential link between CozE proteins and LTA synthesis. To screen for potential functional links between *cozE* and LTA synthesis genes, sgRNAs targeting *ItaS* and *ugtP-ItaA* were made (Fig. 3A, *ugtP* and *ItaA* are in the same operon and are therefore targeted together with CRISPRi). A reduction in growth rate was observed upon depletion of UgtP-LtaA or LtaS in a wild-type background (Fig. S3A). LTA synthesis genes were then knocked down in the  $\Delta\text{cozEa}$  and  $\Delta\text{cozEb}$  genetic backgrounds, to see whether the absence of these genes affected the growth (Fig. S3A). No major effects were evident, although the growth reduction observed in cells depleted of LtaS or UgtP-LtaA appeared to be slightly alleviated in both  $\Delta\text{cozEa}$  and  $\Delta\text{cozEb}$  backgrounds (indicated by the lengths of the red arrows in Fig. S3A). Following up on this, the growth and cell size defects observed upon knockdown of LtaS were indeed less in a  $\Delta\text{cozEb}$  genetic background, although the observed effect was relatively minor (Fig. S4).

Subsequently, we proceeded to investigate the growth phenotypes when both CozEa and CozEb were absent simultaneously with the LTA biosynthesis genes (Fig. 3B; Fig. S3B). Interestingly, when UgtP-LtaA were depleted in a strain lacking both CozE proteins, the growth was improved compared to the control strain only lacking CozE proteins (MDB25 vs MDB11, Fig. 3B; Fig. S3B), suggesting that the detrimental effect of lacking both CozEa and CozEb is partly alleviated when UgtP and/or LtaA is removed. The same trend, although less clear, was also observed when LtaS was depleted in this background (strain MDB26, Fig. 3B; Fig. S3B). Together, these observations suggested potential functional

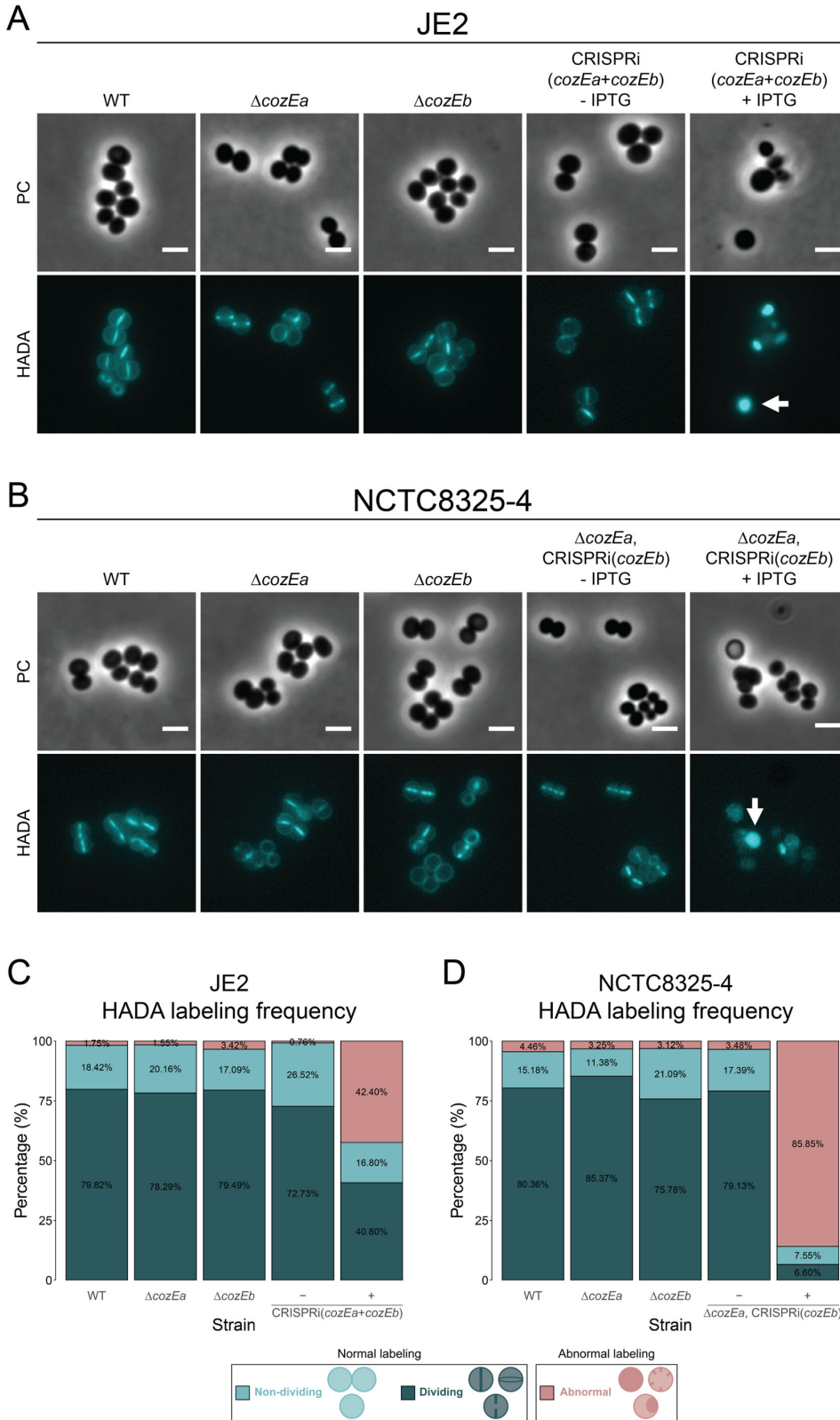


**FIG 2** Localization of peptidoglycan synthesis in *S. aureus* JE2 and NCTC8325-4. (A) Phase contrast (PC) and fluorescence micrographs of HADA-labeled JE2 wild-type (MDB9),  $\Delta\text{cozEa}$  (MDB38),  $\Delta\text{cozEb}$  (MDB10), and CRISPRi(*cozEa + cozEb*) (MDB19). (B) Phase contrast (PC) and fluorescence micrographs of HADA-labeled NCTC8325-4 wild-type (MDB1),  $\Delta\text{cozEa}$  (MDB2),  $\Delta\text{cozEb}$  (Continued on next page)

FIG 2 (Continued)

(MDB3), and  $\Delta\text{cozEa}$ , CRISPRi(*cozEb*) (MDB11). Both JE2 and NCTC8325-4 cells were incubated with HADA for 2 minutes at 37°C. The double *cozE* mutants (MDB19 and MDB11) were grown with and without IPTG. The induced cells displayed irregular HADA staining, indicated by the white arrows. The scale bars are 2  $\mu\text{m}$ . Frequency of cells with normal (dividing and non-dividing) and abnormal HADA labeling for (C) JE2 wild-type (MDB9),  $\Delta\text{cozEa}$  (MDB38),  $\Delta\text{cozEb}$  (MDB10), and CRISPRi(*cozEa* + *cozEb*) (MDB19), and (D) NCTC8325-4 wild-type (MDB1),  $\Delta\text{cozEa}$  (MDB2),  $\Delta\text{cozEb}$  (MDB3), and  $\Delta\text{cozEa}$ , CRISPRi(*cozEb*) (MDB11). The distributions were obtained by manually counting the labeling pattern of 100–150 randomly selected HADA-stained cells from each strain.

links between *CozE* and glycolipid synthesis and prompted us to investigate the interplay between the *cozE* genes and LTA biosynthesis genes *ugtP* and *ltaA*.

### LtaA and UgtP modulate the essentiality of CozE proteins

To further understand how *ugtP-ltaA* knockdown partly alleviated the growth defects of *CozEa* and *CozEb* deficient cells, the sgRNAs targeting *cozEa*, *cozEb*, or both *cozEa* and *cozEb* simultaneously were transformed into *S. aureus* JE2 strains with single deletions of *ugtP* ( $\Delta\text{ugtP}::\text{Tn}$ ) or *ltaA* ( $\Delta\text{ltaA}::\text{Tn}$ ). Both  $\Delta\text{ugtP}$  and  $\Delta\text{ltaA}$  exhibited growth rates comparable to the wild-type strain, and no alterations in growth were observed upon knockdown of the individual *cozE* genes in the JE2  $\Delta\text{ugtP}$  or  $\Delta\text{ltaA}$  cells (Fig. S5). Strikingly, however, simultaneous knockdown of *cozEa* and *cozEb* in  $\Delta\text{ugtP}$  or  $\Delta\text{ltaA}$  background

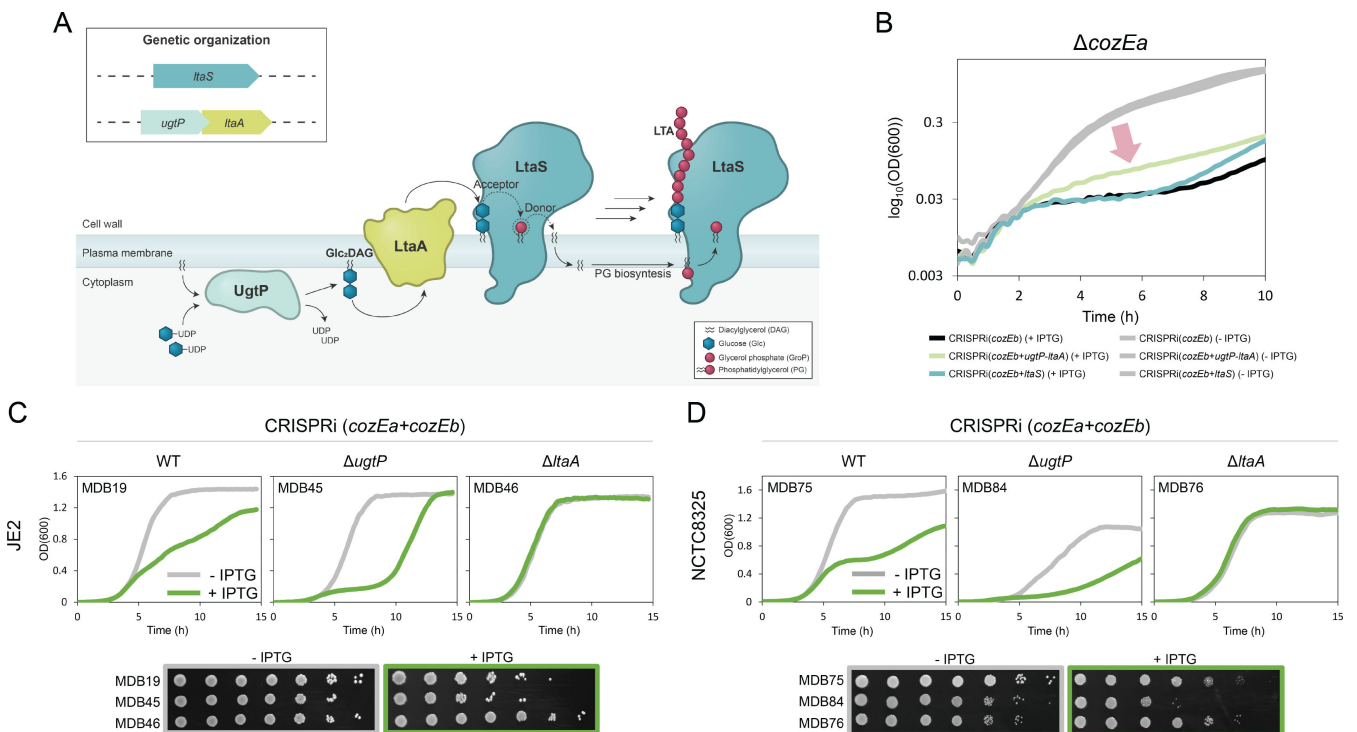


**FIG 3** Synthetic genetic relationships between *cozE* genes and genes involved in LTA biosynthesis. (A) Schematic overview of the LTA biosynthetic pathway. UgtP (also referred to as Ypfp) synthesizes the LTA glycolipid anchor, Glc<sub>2</sub>DAG, from UDP-glucose and diacylglycerol (DAG), which is flipped to the outer membrane leaflet by LtaA. LtaS then synthesizes the LTA polymer by transferring glycerol phosphate units (GroP) derived from phosphatidylglycerol (PG) to the glycolipid anchor. The genetic organization of *ltaS*, *ugtP*, and *ltaA* is indicated in the box. (B) The initial 10 hours of growth for MDB11 [ $\Delta\text{cozEa}$ , CRISPRi(*cozEb*)], MDB25 [ $\Delta\text{cozEa}$ , CRISPRi(*cozEb+ugtP-ltaA*)], and MDB26 [ $\Delta\text{cozEa}$ , CRISPRi(*cozEb+ltaS*)] from Fig. S3 displayed in logarithmic scale to provide a clearer representation of the growth alleviation observed when *ugtP-ltaA* was knocked down together with *cozEb* in the  $\Delta\text{cozEa}$  background (red arrow). The graphs represent averages from triplicate measurements. The CRISPRi strains were grown with and without IPTG, as indicated by the colors. (C and D) Growth of wild-type,  $\Delta\text{ugtP}$ , and  $\Delta\text{ltaA}$  cells with double *cozE* knockdown in (C) JE2 (MDB19, MDB45, and MDB46) and (D) NCTC8325 (MDB75, MDB84, and MDB76) in liquid cultures (top panels) and on agar plates (bottom panels). Cells were grown in the presence or absence of IPTG (15  $\mu\text{M}$  for JE2 and 125  $\mu\text{M}$  for NCTC8325) as indicated by the colors. Strain names are indicated in the figure. The graphs represent averages from triplicate measurements.

caused dramatic but opposite alterations to the growth patterns (partial knockdown in Fig. 3C and full knockdown in Fig. S6A). In the  $\Delta ugtP$  mutant, depletion of the CozE proteins (MDB45) resulted in a synthetic sick phenotype with reduced growth compared to the cells depleted of only the CozE proteins (MDB19) (Fig. 3C; Fig. S6A). On the contrary, in the  $\Delta ltaA$  mutant, depletion of CozE proteins (MDB46) had less a detrimental effect and the growth patterns were more similar to the wild-type (Fig. 3C; Fig. S6A), indicating a synthetic viable genetic interaction.

To further confirm the opposite growth alterations, we conducted the same analysis in *S. aureus* NCTC8325 cells. In contrast to JE2, NCTC8325 (Fig. 3D; Fig. S6B) displayed reduced growth for both  $\Delta ltaA$  and in particular  $\Delta ugtP$ , compared to the wild-type (Fig. 3D), consistent with previous studies noting distinct strain variations in the severity of growth defects associated with these deletions (8, 32). Clearly, however, the same CozE-mediated growth patterns were observed in both strains (Fig. 3D). Double depletion of CozEa and CozEb was detrimental for growth in a wild-type background (MDB75), and while the growth was further reduced in  $\Delta ugtP$  (MDB84), this effect was alleviated in  $\Delta ltaA$  (MDB76) (Fig. 3D; Fig. S6B), confirming that these genetic links are conserved across strains.

Single-cell analyses of the combined mutants further corroborated the pairwise synthetic genetic interactions between *ugtP*, *ltaA*, and *cozE* (Fig. 4; Fig. S7). The mis-regulation of septal synthesis and cell size defects previously observed in cells depleted of both CozE proteins were further elevated in the absence of UgtP, as observed by phase contrast imaging and staining with VanFL (MDB19 and MDB45, Fig. 4A and B). Conversely, in the  $\Delta ltaA$  cells, depletion of CozEa and CozEb did not yield the same morphological abnormalities (MDB46, Fig. 4A), and the cell size distribution in this mutant more closely resembled that of the control strain (MDB46 and MDB44, Fig. 4B). We also stained these cells with DAPI to visualize their nucleoids, as previous observations have demonstrated perturbed DAPI staining in *S. aureus* cells with simultaneous depletion of CozEa and CozEb (Fig. 1B; Fig. S2B) (26). As expected, the highly irregular and distorted DAPI staining pattern was observed when CozE proteins were depleted in the strain lacking UgtP (MDB19 and MDB45, Fig. 4A), but the phenotype was rescued in the  $\Delta ltaA$  background (MDB46 and MDB44, Fig. 4A).

Finally, we performed transmission electron microscopy (TEM) as well as HADA labeling of the same strains. Consistent with previous findings (26), cells lacking both CozE proteins exhibited a large fraction of lysed cells (black arrows in Fig. 4C) in addition to cells with misplaced and abnormal septa (white arrows in Fig. 1G, Fig. 4C and D; Fig. S7A), and this phenotype was further exacerbated in the  $\Delta ugtP$  background (Fig. 4C and D; Fig. S7B). However, in the  $\Delta ltaA$  genetic background, the double *cozE* knockdown had a wild-type-like appearance, with few lysed cells and virtually no misplaced septa (Fig. 4C and D; Fig. S7C). Together, these results show that when UgtP is absent, and Glc<sub>2</sub>DAG is not produced (Fig. 3A), CozE proteins become more essential. On the other hand, when LtaA is absent, and thus the flipping of Glc<sub>2</sub>DAG to the outer membrane leaflet is reduced, the CozE proteins seem to be less functionally important.

### CozEb, but not CozEa, affects LTA polymer length

Previous studies have demonstrated that *S. aureus ugtP* and *ltaA* deletion mutants displayed division defects (14). This has been attributed to the production of abnormally long LTA polymers formed on an alternative lipid anchor in these mutants, as a result of the loss or reduction in Glc<sub>2</sub>DAG on the extracellular leaflet (14, 16). To determine whether CozEa and/or CozEb could influence the LTA polymer in *S. aureus*, the relative lengths of LTA polymers of exponential phase *S. aureus* mutants were analyzed by immunoblotting using an anti-LTA antibody. Notably, the LTA polymers were slightly, but consistently, longer in the  $\Delta cozEb$  mutants compared to the wild-type for both JE2 and NCTC8325-4 (Fig. 5A; Fig. S8A). The LTA size in the  $\Delta cozEa$  mutants, on the other hand, was similar to the wild-type for both strains (Fig. 5A; Fig. S8A). Indeed, complementation experiments further showed that expression of *cozEb*, but not *cozEa*, could recover

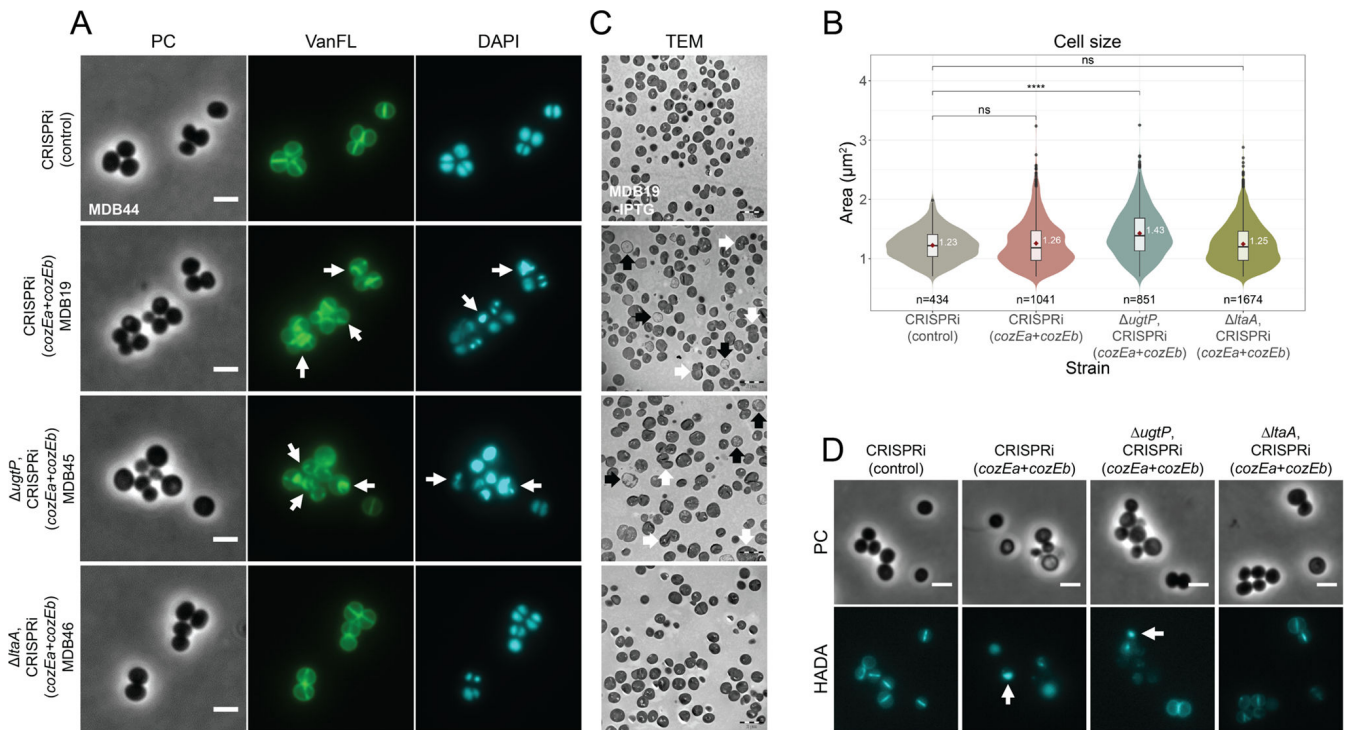


**FIG 4** Morphological analysis of CozE depletion in different genetic backgrounds, wild-type,  $\DeltaugtP$ , and  $\Delta ltaA$ , in *S. aureus* JE2. (A) Micrographs of JE2 CRISPRi(control) (MDB44), CRISPRi(*cozEa + cozEb*) (MDB19),  $\DeltaugtP$ , CRISPRi(*cozEa + cozEb*) (MDB45), and  $\Delta ltaA$ , CRISPRi(*cozEa + cozEb*) (MDB46) showing phase contrast (PC) and fluorescence microscopy of cells stained with the cell wall label VanFL and the nucleoid label DAPI. The cells were grown in a medium with IPTG for induction of the CRISPRi system. White arrows point to cells with perturbed septum formation and abnormal nucleoid staining. The scale bars are 2  $\mu$ m. (B) Violin plots of the cell areas (in  $\mu$ m<sup>2</sup>) of the same cells as in panel A, MDB44 ( $1.23 \pm 0.25 \mu$ m<sup>2</sup>), MDB19 ( $1.26 \pm 0.38 \mu$ m<sup>2</sup>), MDB45 ( $1.43 \pm 0.40 \mu$ m<sup>2</sup>), and MDB46 ( $1.25 \pm 0.35 \mu$ m<sup>2</sup>), determined using MicrobeJ. Significant differences between the strains are indicated with asterisks (\* indicates a *P*-value of <0.05, \*\* indicates a *P*-value of <0.01, and \*\*\* indicates a *P*-value of <0.001, derived from the Mann-Whitney test). The number of cells analyzed for each strain is indicated in the figure. (C) TEM micrographs of uninduced and induced CRISPRi(*cozEa + cozEb*) (MDB19) cells, induced  $\DeltaugtP$ , CRISPRi(*cozEa + cozEb*) (MDB45) cells, and induced  $\Delta ltaA$ , CRISPRi(*cozEa + cozEb*) (MDB46) cells. White arrows point to cells with perturbed septum formation, while black arrows point to lysed cells. The scale bars are 2  $\mu$ m. (D) Phase contrast (PC) and HADA staining micrographs of the same strains as in panels A and B (MDB44, MDB19, MDB45, and MDB46). The cells were incubated with HADA for 2 minutes at 37°C. The strains were grown in the presence of IPTG for induction of the CRISPRi system. The induced wild-type and  $\DeltaugtP$  cells displayed irregular HADA staining, indicated by the white arrows. The scale bars are 2  $\mu$ m.

the LTA to wild-type lengths in the  $\Delta cozEb$  backgrounds (Fig. 5B). We also observed that the LTA size did not increase further in the  $\Delta cozEb$  background when *cozEa* was knocked down (Fig. 5A). The quantity of LTA polymers produced in the cells was not clearly affected in the *cozE* deletion strains, as indicated by similar band intensities in the immunoblots across more than 10 repeated assays (Fig. 5; Fig. S8). Together, these results suggest that CozEb has a unique role in modulating the length of LTA polymers in *S. aureus*, although it should be noted that the increase in LTA polymer length in the *cozEb* mutants appear to be less dramatic than in cells lacking UgtP and/or LtaA (Fig. 5A). In addition, this shows, for the first time, that CozEa and CozEb have distinct functions in *S. aureus*, pointing toward an intricate relationship between the two homologues beyond their redundant, overlapping functions.

### LTA stability is compromised in the absence of CozEb

We also analyzed the presence of LTA in the supernatant fraction of cells lacking CozEa and/or CozEb using the anti-LTA antibody. Detection of LTA in supernatants (which are thus no longer anchored in the cytoplasmic membrane) serves as an indicator of the strength of cell envelope anchoring, referred to in this context as LTA stability. Strikingly, in the JE2  $\Delta cozEb$  mutant, LTA is clearly being released to the growth medium (Fig. 5C;

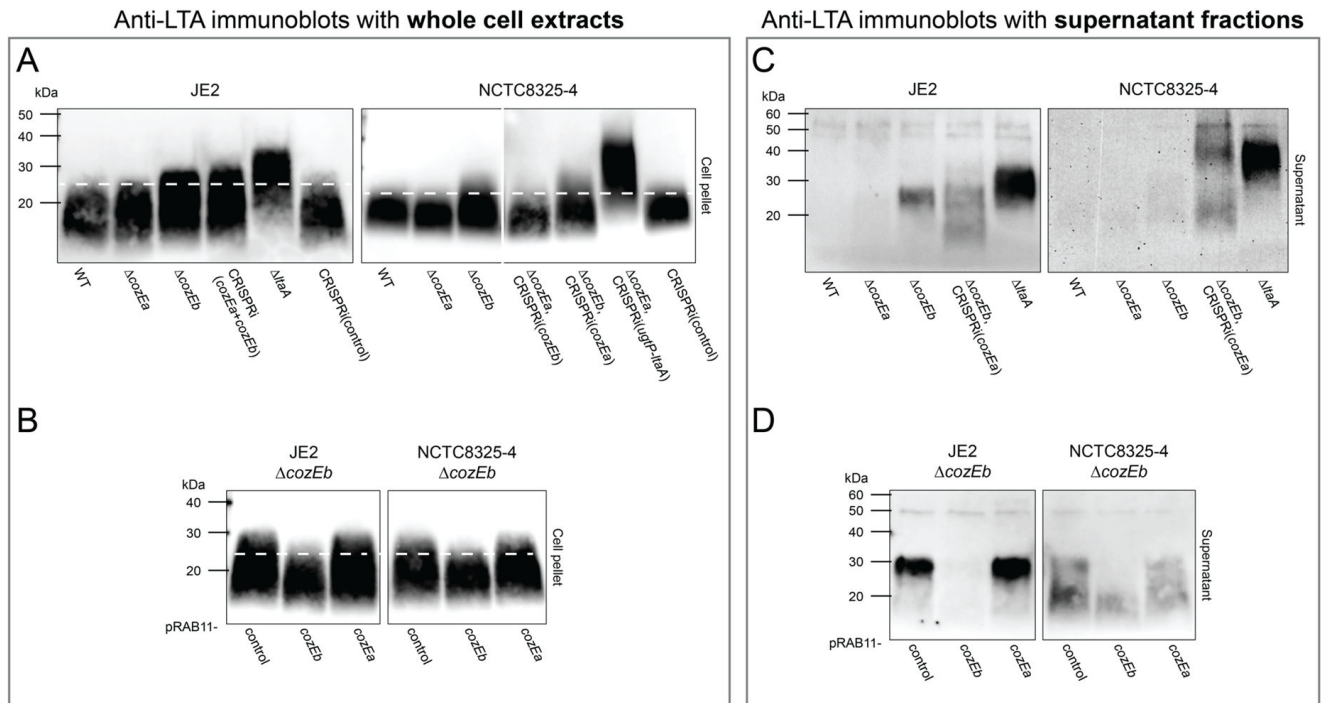


**FIG 5** Characterization of LTA polymer length and stability in single and double *coxE* mutants. LTA polymers were detected in whole-cell extracts (A and B) and in supernatant fractions (C and D) by immunoblotting with an anti-LTA antibody. (A) Immunoblots of wild-type,  $\Delta coxEa$ ,  $\Delta coxEb$ , a double *coxE* mutant, a positive control strain, and a CRISPRi control strain in JE2 (MDB9, MDB38, MDB10, MDB19, MDB40, and MDB44) and NCTC8325-4 (MDB1, MDB2, MDB3, MDB11, MDB12, MDB28, and MM75). (B) Complementation experiments in JE2 (MDB61, MDB60, and MDB59) and NCTC8325-4 (MDB63, MDB62, and MDB58). The plasmids pRAB11-*coxEb* and pRAB11-*coxEa*, as well as a pRAB11 control plasmid, were introduced into the  $\Delta coxEb$  mutants. Expression of the plasmid-located genes was induced by the addition of 0.004  $\mu\text{g}/\text{mL}$  aTc. Panels A and B illustrate that LTA polymers are consistently longer in the absence of CozEb and that this phenotype can be complemented with ectopic expression of CozEb but not CozEa. (C) Immunoblots of wild-type,  $\Delta coxEa$ ,  $\Delta coxEb$ , a double *coxE* mutant, and a positive control strain in JE2 (MDB9, MDB38, MDB10, MDB21, and MDB40) and NCTC8325-4 (MDB1, MDB2, MDB3, MDB12, and MDB69). (D) Complementation experiments in JE2 (MDB176, MDB60, and MDB59) and NCTC8325-4 (MDB174, MDB62, and MDB58). The plasmids pRAB11-*coxEb* and pRAB11-*coxEa*, as well as a pRAB11 control plasmid, were introduced into the  $\Delta coxEb$  mutants. Expression of the plasmid-located genes was induced by the addition of 0.004  $\mu\text{g}/\text{mL}$  aTc. Panels C and D illustrate that the stability of LTA polymers is compromised in the absence of CozEb and that it can only be recovered with ectopic expression of CozEb, not CozEa.

Fig. S8B), while no LTA is detected in the supernatant fraction of wild-type or  $\Delta coxEa$ . Although less clear, the same trend is also seen in NCTC8325-4 (Fig. 5C; Fig. S8B). Furthermore, complementation experiments showed that expression of *coxEb*, but not *coxEa*, fully recovered the LTA stability in the JE2  $\Delta coxEb$  background and partial rescue was observed for NCTC8325-4 (Fig. 5D). The size of the released LTA polymers corresponds to the LTA with increased length in the  $\Delta coxEb$  mutant (Fig. S8C), suggesting that only the abnormally long LTA polymers are unstable and consequently released into the growth medium. A  $\Delta ltaA$  mutant, which has previously been shown to release LTA (33), was included as a control in this experiment, and as expected LTA polymers with increased size were detected in the supernatant of this strain. For the double *coxE* mutants [ $\Delta coxEb$ , CRISPRi(*coxEa*)], LTA with a range of sizes was detected in the supernatant. This observation can probably be attributed to the high degree of lysis observed in these double mutants (Fig. 4C), which likely leads to the release of LTA to the supernatant. Collectively, these findings suggest that CozEb has a role in modulating the stability, as well as the length, of LTA polymers in *S. aureus*.

LTA functions as a docking molecule for the major autolysin Atl and contributes to the regulation of autolysin activity in *S. aureus* (4, 34). Staphylococcal cells lacking LTA ( $\Delta ltaS$ ) exhibit reduced autolysis (4, 14), whereas those with long and abnormal LTA polymers ( $\Delta ltaA$  and  $\Delta ugtP$ ) are more autolytic (6, 14). Autolysis assays indeed showed that

NCTC8325-4  $\Delta$ *cozEb* displayed increased susceptibility to lysostaphin and Triton X-100 (Fig. S9). For JE2, however,  $\Delta$ *cozEb* showed similar autolytic behavior as the wild-type (Fig. S9). Together, these results further support the role of CozEb in LTA biosynthesis, although the phenotypes are different between strains.

### CozE proteins are not critical for the membrane localization of UgtP

Next, we asked how CozE proteins could influence the LTA biosynthetic pathway. First, we studied their subcellular localization in detail using strains with chromosomally integrated *cozEa-gfp* and *cozEb-gfp* fusions in their native loci in NCTC8325-4 (MK1582 and MK1584, respectively, Fig. S10). Immunoblotting using an anti-GFP antibody demonstrated that the two fusion proteins (67.03 kDa for CozEa-GFP and 71.93 kDa for CozEb-GFP) have relatively similar expression levels (Fig. S10A). The fluorescence microscopy analysis revealed an uneven and spotty localization of both CozE proteins in the membrane, without any septum enrichment, similar to what has been reported for CozEb in *S. pneumoniae* (24) (Fig. S10B). Interestingly, time-lapse microscopy revealed that the spotty localization is highly dynamic, indicating that both CozEa-GFP and CozEb-GFP move rapidly around in the cell membrane (see the arrows in Fig. S10C; Movie S1 and S2). While LtaA has been shown to localize uniformly in the membrane, a somewhat spotty membrane localization was reported for UgtP (19). The mechanism of membrane localization for UgtP, a 391 amino acid-long protein without any predicted transmembrane segments, is not established (19), and we therefore asked whether CozE proteins could be involved in this process. A strain with a chromosomally integrated ectopic copy of *gfp-ugtP* expressed from its native promoter was made, and as expected GFP-UgtP displayed a spotty localization in the membrane (Fig. S11A). Membrane-enriched localization of GFP-UgtP was still observed in all of the *cozE* knockdown strains, although the fraction of cells with membrane-localized UgtP was slightly reduced when CozEb was absent (Fig. S11B). Split luciferase assays were performed to identify potential protein-protein interactions; however, the results did not reveal any direct interaction between UgtP and the CozE proteins (Fig. S11C through E). Together, this indicates that neither CozEa nor CozEb are directly responsible for the cellular localization of UgtP.

### CozE proteins modulate LtaA-mediated flipping of Glc<sub>2</sub>DAG

With the same split luciferase assay as above, we also tested the potential interaction between CozE proteins and LtaA. Indeed, both CozE proteins appear to interact directly with LtaA (Fig. S11C through E). Our results above showed that the absence of LtaA (implying that the translocation of Glc<sub>2</sub>DAG across the membrane is impaired) altered the functional relevance of the CozE proteins. Thus, we asked whether the presence of CozEa and/or CozEb could influence the LtaA-mediated flipping of Glc<sub>2</sub>DAG. To answer this question, we performed *in vitro* flipping assays with LtaA proteoliposomes reconstituted alone (35) or in the presence of CozEa and/or CozEb (Fig. 6; Fig. S12). Fluorescently labeled Glc<sub>2</sub>DAG (diglucosyl-diacylglycerol-NBD) was also incorporated in the proteoliposomes as a reporter of flipping activity (Fig. 6A). Glc<sub>2</sub>DAG-NBD in the outer leaflet undergo fluorescence quenching upon the addition of the membrane-impermeable reducing agent sodium dithionite, and the extent of flipping can therefore be determined by measuring the percentage of fluorescence remaining after sodium dithionite addition (Fig. 6A). Our results indicate that CozEb, but not CozEa, decreases LtaA flipping activity *in vitro* (Fig. 6B). Interestingly, when CozEa is present, the effect of CozEb is abrogated, thus protecting LtaA from the apparent inhibitory effect of CozEb (Fig. 6B).

## DISCUSSION

In line with previous observations in *S. aureus* SH1000 (26), we here show that *cozEa* and *cozEb* constitute a synthetic lethal gene pair across *S. aureus* strains. Cell cycle analyses of CozE-depleted strains show an enrichment of cells without septa (phase 1), and the

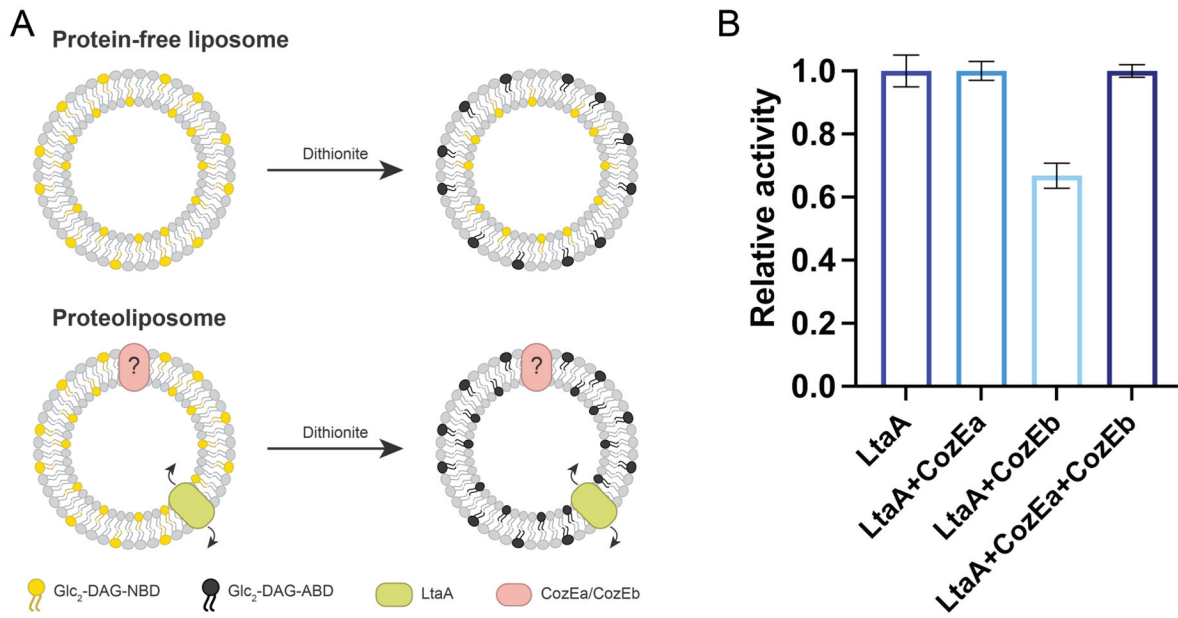


**FIG 6** LtaA-catalyzed Glc<sub>2</sub>DAG flipping in the presence of CozE proteins. (A) Schematic overview of the *in vitro* flipping assay. Liposomes are reconstituted with NBD-labeled Glc<sub>2</sub>DAG LTA anchors (yellow) that distribute equally in the two membrane leaflets. The fluorescently labeled LTA anchors undergo fluorescence quenching (black) upon the addition of sodium dithionite, causing 50% fluorescence loss in protein-free liposomes due to the reduction of only the outer-leaflet fluorophores. However, when LtaA (green), known to facilitate the translocation of Glc<sub>2</sub>DAG across the membrane, is present, a larger proportion of the fluorophores are reduced due to the flipping activity of LtaA. (B) Relative activity of LtaA in the presence of CozE proteins. Relative activity = 100 × (F<sub>i</sub> – F<sub>liposomes</sub>) / (F<sub>LtaA</sub> – F<sub>liposomes</sub>), where *i* corresponds to each set of proteoliposomes, *liposomes* correspond to the fluorescence at the plateau for protein-free liposomes, and F<sub>i</sub> corresponds to the fluorescence at the plateau for proteoliposomes containing (i) LtaA; (ii) LtaA and CozEa (1:1 molar ratio); (iii) LtaA and CozEb (1:1 molar ratio); and (iv) LtaA, CozEa, and CozEb (1:1:1 molar ratio). Error bars show ± s.d. of technical replicates, *n* = 3.

aberrant localization of cell wall and peptidoglycan synthesis in these cells provides additional validation for their effect on cell division and septum formation in *S. aureus*. The effect of CozE proteins on morphology and growth has consequently directed most studies of these proteins toward their direct interaction with the cell wall and cell division synthesis machinery (21, 24–26, 36). In the present study, we have made discoveries that link the function of these proteins to LTA biosynthesis in *S. aureus*. It is indeed well established that mutants of *ugtP*, *ltaA*, and *ltaS* cause cell division defects (4, 8, 14). CozEa/CozEb do not interact with any of the PBPs found in *S. aureus* (26). However, LTA biosynthetic proteins are shown to associate with a number of proteins involved in cell wall synthesis and division, including PBP1, PBP2, PBP3, FtsW, EzrA, DivIB, DivIC, and FtsL (19). Furthermore, it has been demonstrated that LTA affects the activity of cell wall hydrolases/autolysins required for proper cell splitting (14, 37). In this context, the findings presented in this study suggest that the cell division phenotypes associated with CozE proteins in *S. aureus* may, at least to some extent, be attributed to the effect they have on the LTA biosynthetic pathway (26, 38), although other mechanisms, such as their direct interaction with EzrA (26) or more general effect on membrane homeostasis (see below) may also play a role.

Our data demonstrate an intricate interplay between CozE proteins and the LTA biosynthetic pathway in *S. aureus*. First, it was noted that the mutants lacking both CozE proteins (Fig. 1; Fig. S2) were phenotypically similar to staphylococcal cells lacking LTA biosynthetic genes (6, 7, 14). Second, our genetic analyses demonstrated that the essentiality of CozE proteins is altered in the absence of LTA biosynthetic genes. Particularly interesting, when the flippase encoding gene *ltaA* is deleted, resulting in accumulation of the glycolipid anchor Glc<sub>2</sub>DAG on the intracellular membrane leaflet and reduced levels of Glc<sub>2</sub>DAG on the extracellular leaflet, the essentiality of CozE proteins appears to be alleviated (Fig. 3 and 4). The opposite seems to be true for

*ΔugtP*. In these cells, where the glycolipid anchor is lacking completely, the absence of CozEa and CozEb results in an aggravated growth defect compared to the wild-type background (see further discussion below). In line with these genetic links, suppressor mutations in *cozEb* have previously been reported in a *ΔltaS* mutant (12). Third, we here observed that deletion of CozEb resulted in slightly longer and more unstable LTA polymers compared to the wild-type (Fig. 5; Fig. S8), although the latter phenotype is somewhat strain-dependent. This effect has previously been associated with cells lacking (*ΔugtP*) or having reduced levels of (*ΔltaA*) the LTA anchor Glc<sub>2</sub>DAG on the extracellular leaflet (16). In the absence of Glc<sub>2</sub>DAG, PG can be used as an alternative starter unit for LTA synthesis (6), and LTA polymers formed on PG are longer and more unstable than those formed on Glc<sub>2</sub>DAG (16). It is likely that the effect of CozEb on LTA length and stability is due to different LTA anchors being used in the mutants. However, it remains enigmatic why the growth and cell division phenotypes are observed only in the double *cozE* mutants, while CozEb alone clearly affects LTA.

In *S. pneumoniae*, CozE proteins are involved in spatiotemporal localization of peptidoglycan synthesis, probably through their interaction and control of the bifunctional class A PBP (21, 25). The link between CozE proteins and teichoic acids observed in *S. aureus* may however be relevant also in this species. It has, for example, been shown that the growth reduction caused by *cozE* knockdown in *S. pneumoniae* is improved in a mutant where the "LTA anchor formation protein B" gene (*lafB*, also named *cpoA*, involved in the synthesis of glycolipid Gal-Glc-DAG) is deleted (39). Furthermore, in a *S. pneumoniae* *taeL* (encoding the lipoteichoic acid ligase required for LTA assembly) deletion mutant, suppressors in *cozE* were found (40).

It still remains to be fully understood how CozE proteins influence LTA. CozE proteins modulate the flipping activity of LtaA, as demonstrated by *in vitro* assays (Fig. 6). The bilayer distribution of Glc<sub>2</sub>DAG LTA anchor in the membrane may therefore be changed in *cozE* mutant cells, thus disturbing the synthesis of LTA polymers, as observed in the *ΔcozEb* background. The protein-protein interactions observed between LtaA and both CozE proteins *in vivo* suggest that CozE proteins may directly affect the LtaA function. However, we cannot exclude that CozE proteins influence LTA anchor flipping independently of LtaA since proteoliposomes without LtaA were not analyzed. It is also possible that CozE proteins have a more general effect on membrane homeostasis, for example by altering the overall lipid composition or distribution/production of membrane vesicles. In fact, labeling of cells with Nile Red revealed membrane alterations in double *cozE* mutants compared to the wild-type and single *cozE* mutants (Fig. S13). Notably, these membrane staining defects were not apparent in any of the LTA biosynthesis mutants, suggesting that CozE proteins may play a role in membrane homeostasis beyond LTA biosynthesis. It is also interesting to note that both CozEa and CozEb are highly dynamic membrane proteins, and it could be speculated that their role is important not only for the flipping of lipids but also for the lateral dynamics of lipids and/or fluidity of the membrane. Also worth noting in this context is that a *ΔcozEb* mutant in *S. pneumoniae* has been shown to display increased susceptibility to the membrane-targeting antibiotic daptomycin (36, 41, 42). Furthermore, our results show that the essentiality of CozE proteins is oppositely affected in *ΔltaA* and *ΔugtP* backgrounds (Fig. 3), suggesting that CozE proteins may be involved in the bilayer distribution of lipids. Alongside flippases, which actively translocate lipids across membranes, lipid scramblases, membrane proteins which facilitate passive, bidirectional translocation of lipids between membrane leaflets, are known to play important functions in regulating lipid distributions in eukaryotic cells (43). It is tempting to speculate that CozE proteins function as bacterial membrane scramblases, and in that way affect many membrane-associated processes including peptidoglycan and teichoic acid biosynthesis. However, this hypothesis needs further investigation, for example by structural analysis of potential interactions between the highly dynamic CozE proteins and different lipids and/or by analyzing the distribution of lipids between the bilayers in different genetic backgrounds.

Our results also demonstrate that CozEa and CozEb are not fully redundant in *S. aureus*, as deletion of *cozEb*, but not *cozEa*, resulted in longer and more unstable LTA polymers (Fig. 5). This is not entirely surprising given the different roles of the two CozE paralogs in *S. pneumoniae* (25). The notion of the unique functionality of these paralogs is indeed supported by a phylogenetic analysis of CozE proteins from *Streptococcaceae* (25) and *Staphylococcaceae* (Fig. S14). The phylogenetic analysis of CozE from 28 different species within the *Staphylococcaceae* family demonstrated that each species encodes two CozE proteins and that the two paralogs cluster into two separate subgroups, corresponding to CozEa and CozEb (blue and red, respectively, in Fig. S14) for the genera *Staphylococcus* and *Macrococcus*. It should be noted that CozE proteins from more distantly related genera (*Jeotgalicoccus*, *Salinicoccus*, and *Nosocomiicoccus*) do not display this subclassification, but instead cluster into a separate group that is phylogenetically closer to CozEa (green in Fig. S14), indicating that the function of CozEb may be unique for *Staphylococcus* and *Macrococcus*.

It has already been shown that CozEb can act as a target for antibody-based infection treatment in *S. pneumoniae* (36). Functional insights into the role of CozE proteins in different bacteria are needed to further explore their potential in anti-microbial or anti-infection treatment. The novel functions of CozE proteins demonstrated here reveal that these proteins are new players in the control of LTA biosynthesis and membrane homeostasis in *S. aureus*. Future work should aim at further deciphering the interplay between the CozE proteins and between CozE proteins and LTA synthesis, membrane homeostasis, and cell division in *S. aureus* and other bacteria.

## MATERIALS AND METHODS

### Bacterial strains and growth conditions

Strains used in this work are listed in Table S1. *S. aureus* strains NCTC8325-4, NCTC8345, and JE2-USA300 (called JE2 here) were grown in BHI medium with shaking or on BHI agar plates at 37°C, if not stated otherwise. *E. coli* strains IM08B and BL21-Gold (DE3) were grown in LB medium with shaking or on LA plates at 37°C, if not stated otherwise. When appropriate, antibiotics were added for selection: 100 µg/mL ampicillin and/or 25 µg/mL chloramphenicol for *E. coli*, 100 or 1,000 µg/mL spectinomycin (for NCTC8325-4 and JE2, respectively), 5 µg/mL erythromycin and/or 10 or 25 µg/mL chloramphenicol for *S. aureus*. Isopropyl β-D-1-thiogalactopyranoside (IPTG) and anhydrotetracycline (aTc) were added for induction of transcription when needed.

For the transformation of *E. coli*, chemically competent IM08B cells were prepared using calcium-chloride treatment followed by transformation with heat shock according to standard protocols. *S. aureus* strains were transformed by electroporation with plasmids isolated from *E. coli* IM08B, as described previously (44).

### Strain construction

All strains used in this work are listed in Table S1, plasmids are listed in Table S2 while primers used for the cloning are listed in Table S3. Every construct was verified by PCR and sequencing.

#### Deletion of *cozEa* and *cozEb* ( $\Delta\text{cozEa}::\text{spc}$ and $\Delta\text{cozEb}::\text{spc}$ )

Deletion of *cozEa* or *cozEb* in *S. aureus* NCTC8325-4 was achieved using the temperature-sensitive pMAD system, following the same approach as described before (26).

#### Deletion of *ugtP* ( $\Delta\text{ugtP}::\text{spc}$ )

Deletion of *ugtP* in *S. aureus* NCTC8325 was achieved using the temperature-sensitive pMAD system. To construct pMAD- $\Delta\text{ugtP}::\text{spc}$ , three DNA fragments were initially amplified: (i) the *ugtP* upstream sequence (“ugtP\_up”) (ii), a spectinomycin resistance cassette (“spc”), and (iii) the *ugtP* downstream sequence (“ugtP\_down”), using primers

listed in Table S3. gDNA from *S. aureus* NCTC8325-4 served as template DNA for the amplification of both *ugtP*\_up and *ugtP*\_down, while the pCN55 plasmid (45) was used as the template for the amplification of *spc*. The primers were designed with overlapping sequences, enabling the fusion of the three fragments by overlap extension PCR. The resulting fragment was digested with BamHI (introduced with the outer primer mk506) and NcoI (naturally occurring near the 5' end of the fragment) and subsequently ligated into the corresponding sites of pMAD. The generated plasmid was verified by PCR and sequencing, and the standard pMAD protocol (29) was used to replace *ugtP* with the *spc*-marker. Note that the *ugtP*-fragment was amplified without any terminator sequence to avoid any downstream effects on the transcription of *ltaA*.

### Construction of CRISPR interference strains

For knockdown of genes, the two-plasmid CRISPR interference system described previously (26, 30) was used. In this system, the appropriate strains are transformed with a plasmid carrying an IPTG-inducible *dcas9* (pLOW-*dcas9*) and another plasmid carrying a gene-specific sgRNA with constitutive expression [pCG248-sgRNA(*xxx*) or pVL2336-sgRNA(*xxx*), where *xxx* denotes the target gene]. The sgRNA plasmids were constructed using inverse PCR in pCG248 (26) or Golden Gate cloning in pVL2336 (30), using oligos listed in Table S3, and verified by PCR and sequencing.

### Construction of pRAB11 plasmids used for complementation

The genes of *cozEa* and *cozEb* were initially amplified from *S. aureus* SH1000 gDNA with primers containing KpnI and EcoRI restriction sites as overhangs (see Table S3). Purified PCR products and the plasmid pRAB11 (46) were digested with KpnI and EcoRI and subsequently ligated using T4 DNA Ligase. Ligation mixtures were transformed into *E. coli* IM08B, and the plasmids were verified by PCR and sequencing before being electroporated into *S. aureus*.

### Construction of chromosomally integrated *cozEa-gfp* and *cozEb-gfp* fusions

The temperature-sensitive pMAD system was used to GFP-tag *cozEa* and *cozEb* in their native loci in *S. aureus* NCTC8325-4. For construction of pMAD-*cozEa-m(sf)gfp\_spc*, the *cozEa-gfp* fusion was amplified from plasmid pLOW-*cozEa-m(sf)gfp* using primers mk432 and mk433, while the spectinomycin resistance cassette spliced with the *cozEa* downstream region was amplified from plasmid pMAD-*cozEa::spc* using primers mk188 and mk434. The two fragments were fused by overlap extension PCR and ligated into pMAD using the NcoI and Sall restriction sites introduced with the primers. Similarly, for pMAD-*cozEb-m(sf)gfp\_spc*, the *cozEb-gfp* fusion was amplified from plasmid pLOW-*cozEb-m(sf)gfp* using primers mk435 and mk433, while the *spc* cassette spliced with the *cozEb* downstream region was amplified from plasmid pMAD-*cozEb::spc* using primers mk188 and mk436. These two fragments were also fused by overlap extension PCR and ligated into pMAD using the NcoI and Sall restriction sites introduced with the primers. Finally, a standard pMAD protocol (29) was used for chromosomal integration of the generated fusions.

### Construction of a chromosomally integrated *gfp-ugtP* fusion

A *gfp-ugtP* fusion gene, driven by the *ugtP*-promoter, was integrated into a neutral locus (between genes SAOUHSC\_03046 and SAOUHSC\_03047) on the *S. aureus* NCTC8325-4 chromosome using the temperature-sensitive pMAD system. To construct the plasmid pMAD-P<sub>ugtP</sub>-*m(sf)gfp-ugtP\_spc*, *gfp* was first fused to the 5' ends of *ugtP* by restriction cloning. *ugtP* was amplified using gDNA from *S. aureus* NCTC8325-4 as a template and ligated into the NcoI and BamHI restriction sites of pLOW-*m(sf)gfp*-SA1477 to produce plasmid pLOW-*m(sf)gfp-ugtP*. The four fragments constituting the insert of the pMAD-P<sub>ugtP</sub>-*m(sf)gfp-ugtP\_spc* plasmids were then amplified: (i) the upstream integration region ("ori\_up"), (ii) the *ugtP*-promoter ("P<sub>ugtP</sub>"), (iii) the *gfp-ugtP* fusion

gene (“gfp-ugtP”), and (iv) a spectinomycin resistance cassette spliced with the DNA sequence of the downstream integration region (“*spc +ori\_down*”). Both *ori\_up* and *P<sub>ugtP</sub>* were amplified using gDNA from *S. aureus* NCTC8325-4 as template, while purified pLOW-*m(sf)gfp-ugtP* and pMAD-*ori-parS* were used as template DNA for amplification of *gfp-ugtP* and *spc +ori\_down*, respectively. All primers used for the aforementioned amplifications are listed in Table S3. The four fragments were subsequently spliced by overlap extension PCR and ligated into pMAD, using the EcoRI and Sall restriction sites introduced with the outer primers. Finally, a standard pMAD protocol (29) was used to integrate the generated fusion into the chromosome of *S. aureus* NCTC8325-4.

### Construction of split luciferase plasmids

To C-terminally fuse CozEa and CozEb to SmBit, *cozEa* and *cozEb* were amplified from NCTC8325-4 genomic DNA using the primer pairs *mdb72/mdb73* and *mdb74/mdb75*, respectively. The vectors pAF256-*P<sub>tet</sub>-hupA-smbit/lgbit* and pAP118-*P<sub>tet</sub>-hupA-smbit/hupA-lgbit*, along with the amplified fragments, were then digested with SpeI and BamHI. The digested fragments were ligated into the vectors and subsequently transformed into *E. coli*. The resulting pAF256 vectors, encoding CozE fused to SmBit and LgBit, not part of a fusion protein, were used as negative controls in the split luciferase assays. The pAP118 vectors, on the other hand, were further modified to C-terminally fuse UgtP or LtaA to LgBit. *ugtP* and *ltaA* were amplified from NCTC8325-4 genomic DNA using the primer pairs *mdb80/mdb81* and *mdb82/mdb83*, respectively. The amplified fragments and the vectors pAP118-*P<sub>tet</sub>-cozEa-smbit/hupA-lgbit* and pAP118-*P<sub>tet</sub>-cozEb-smbit/hupA-lgbit* were then digested with PvuI and NotI, and the digested fragments were ligated into the vectors and transformed into *E. coli*. All constructs were verified by PCR and sequencing.

### Construction of pET19b-cozEa and pET19b-cozEb

*cozEa* and *cozEb* was amplified with the primer pairs *mk508/mk509* and *mk510/mk512*, respectively, producing fragments with flanking SpeI and BamHI restriction sites introduced in the primers. The vector LtaA-pET19b and the fragments were digested with SpeI and BamHI, and the digested fragments were ligated into the vector and transformed into *E. coli*. The constructs were verified by PCR and sequencing.

### Growth assays in liquid media

To measure growth in a liquid medium, the bacterial strains to be monitored were initially grown overnight in the BHI medium with the respective antibiotics. They were then diluted 1:1,000 in fresh BHI medium supplemented with the respective antibiotics and inducers, when appropriate. The bacterial dilutions were applied to a 96-well microtiter plate and incubated in a plate reader at 37°C for 18–20 hours. OD<sub>600</sub> measurements were taken every 10 minutes, with a brief shaking of the plate for 2–5 seconds before each measurement. All growth curves in this work are the mean value of three replicate measurements, and they are all representative of at least three independent experiments.

### Spotting assays

To assess growth on solid medium, cells grown overnight in BHI medium were serially 10-fold diluted in fresh BHI medium with antibiotics and IPTG for induction, when appropriate. Each overnight culture and its serial dilutions were spotted onto the appropriate BHI agar plates with a volume of 2 µL. The plates were incubated aerobically at 37°C for 17 to 20 hours. Images of the plates were captured using a Gel Doc XR +Imager (Bio-Rad Laboratories).

## Autolysis assays

Overnight cultures were diluted to an OD<sub>600</sub> of 0.1 in 20 mL TSB, supplemented with the respective antibiotics and inducers, and incubated until their OD<sub>600</sub> reached approximately 0.4. The cells were then harvested by centrifugation, washed with PBS, and resuspended to an OD<sub>600</sub> of 2 in PBS. 100 µL of the cell suspensions were mixed with an equal volume of PBS containing either 200 ng/mL lysostaphin or 0.1% Triton X-100 in a 96-well plate. OD<sub>600</sub> readings were taken every 10 minutes for 6 hours in a plate reader at 37°C (for lysostaphin) or 30°C (for Triton X-100). Lysis was determined as the decrease in OD<sub>600</sub> over time and presented as the average percentage of the initial OD from four technical replicates. The data shown in this work are representative of at least two independent experiments.

## Epifluorescence- and phase contrast microscopy

For microscopy analyses, strains were first grown overnight in a BHI medium with the respective antibiotics. The overnight cultures were diluted 1:1,000 in fresh BHI medium containing relevant antibiotics and inducers, and incubated until their OD<sub>600</sub> reached approximately 0.4. In some cases, the cells were stained with fluorescent vancomycin (VanFL, in which a BODIPY fluorophore is linked to a vancomycin molecule [Invitrogen]), DAPI (Invitrogen), and/or Nile Red (Sigma-Aldrich), at final concentrations of 0.8 µg/mL, 7.5 µg/mL, and 3 µg/mL, respectively. In other cases, the cells were stained with a fluorescent D-alanine analog, HADA (31), at a final concentration of 250 µM. The cultures containing HADA were incubated at 37°C for 2 minutes, before being immediately put on ice to stop bacterial growth. The cells were lastly washed with PBS buffer to remove excess unbound dye. Bacterial cells were immobilized on agarose pads (1.2%) before imaging on a Zeiss Axio Observer microscope with ZEN Blue software. The bacteria were visualized with a 100× phase contrast objective, and images were captured using an ORCA-Flash4.0 V3 Digital CMOS camera (Hamamatsu Photonics K.K.). Time-lapse (TL) images of cells expressing GFP fusions were acquired every third second for 27 seconds using the aforementioned equipment.

The distribution of cell sizes among different *S. aureus* strains was determined using MicrobeJ (47). Particles of the strain to be analyzed were detected using a stack of phase contrast images of the given strain in MicrobeJ, every image was subsequently corrected manually by discarding and/or adding cells that were incorrectly detected. In addition to analyzing cell sizes, the cell cycle phases of the bacteria were also analyzed by manually counting the different cell phases (phase 1, 2, or 3) of 100–150 randomly selected VanFL-stained cells from each strain. Cell wall synthesis was also analyzed by manually counting the HADA labeling patterns (non-dividing, dividing, or abnormal) of 100–150 randomly selected cells from each strain. All the microscopic images in this work are representative of at least two independent experiments.

## Transmission electron microscopy

The bacterial strains to be visualized by TEM were first grown overnight in BHI medium with the respective antibiotics and then diluted 1:1,000 in fresh BHI with antibiotics and IPTG added when necessary. The diluted bacterial cultures were incubated at 37°C until they reached an OD<sub>600</sub> of 0.3. Each of the bacterial cultures (10 mL) was carefully mixed with 10 mL fixation solution, giving final concentrations of 2% (vol/vol) paraformaldehyde, 0.1 M cacodylate (CaCo) buffer, and 1.25% (vol/vol) glutaraldehyde solution (grade I). The fixation mixtures were incubated at room temperature for 1 hour, followed by incubation at 4°C overnight. The next day, the cells were centrifugated at 5,000 × *g* at 4°C for 5 minutes, and subsequently washed three times with PBS, pH 7.4, and three times with a 0.1 M CaCo buffer. The cells were then post-fixed for 1 hour with 1% OsO<sub>4</sub> in 0.1 M CaCo. The CaCo-washing steps were repeated prior to dehydration, which involved 10-minute incubation steps at increasing concentrations of ethanol (70%, 90%, 96%, and 100%). The samples were next infiltrated with LR White resin by multiple incubation

steps with an increasing concentration of the embedding media (mixed with EtOH). First, overnight with a 1:3 ratio of LR White to EtOH, second; approximately 4 hours with a 1:1 ratio, third; 4 hours with a 3:1 ratio, and finally overnight with 100% LR White. The samples were then embedded in 100% LR White overnight at 60°C by polymerizing the embedding media into a hard block. All sample blocks were sectioned, 60 nm thin, and stained with uranyl acetate and potassium permanganate. A FEI Morgagni 268 Transmission electron microscope was used to analyze the samples. Images of the bacteria were captured using a Veleta CCD camera (Olympus Corporation) with an exposure time of ~1,000 ms.

### Immunoblot analysis of lipoteichoic acid in whole cell extracts and supernatants

Overnight cultures were diluted 1:1,000 in TSB medium with antibiotics and IPTG for induction, when appropriate, and incubated at 37°C until they reached an OD<sub>600</sub> between 0.6 and 0.8. The cultures were normalized to an OD<sub>600</sub> of 0.6 and then harvested by centrifugation at 5,400 × *g* for 3 min at 4°C. Detection of LTA was done essentially as described before (14, 33). The supernatants from each strain were transferred to clean tubes, separating them from the pellets, for individual analysis. For pellet fraction analysis, the pellets were resuspended in 50 μL lysis buffer, containing 50 mM Tris-HCl (pH 7.4), 150 mM sodium chloride, and 200 μg/mL lysostaphin, before incubation at 37°C for 10 minutes. The suspensions were then added to 50 μL 4 × SDS loading buffer and heated at 95°C for 30 minutes. The cell lysates were subsequently centrifuged at 16,000 × *g* for 10 minutes to pellet cellular debris. The supernatants (60 μL) were transferred to clean tubes containing 60 μL dH<sub>2</sub>O. The diluted suspensions were lastly treated with 0.5 μL proteinase K (20 mg/mL) for 2 hours at 50°C. For supernatant fraction analysis, the supernatants were centrifuged at 16,000 × *g* for 10 minutes, 75 μL of each supernatant was mixed with 25 μL 4 × SDS loading buffer and heated at 95°C for 30 minutes. They were subsequently centrifuged at 16,000 × *g* for 10 minutes, and the supernatants (60 μL) were lastly transferred to clean tubes.

The pellet and supernatant samples were separated with SDS-PAGE using a 4-20% Mini-PROTEAN TGX acrylamide gel (Bio-Rad). Next, blotting onto a PVDF membrane was performed using a Trans-Blot Turbo System (Bio-Rad). Afterward, the membrane was blocked in a PBST solution containing 5% (wt/vol) skimmed milk powder for 1 hour at room temperature. After washing with PBST, the membrane was then incubated for 1 hour with an anti-LTA primary antibody (Hycult) (diluted 1:4,000 in PBST). Next, the membrane was washed three times with PBST to remove unbound antibodies and then incubated for another hour with an anti-mouse IgG HRP-conjugate secondary antibody (Promega) (diluted 1:10,000 in PBST). After incubation, unbound antibodies were once again removed by washing the membrane three times with PBST. Finally, the membrane was developed using the SuperSignal West Pico PLUS Chemiluminescent Substrate kit (Thermo Fisher Scientific), and blot images were captured with an Azure Imager c400 (Azure Biosystems).

### Western blot analysis of the relative expression of GFP-tagged CozEa and CozEb

Overnight cultures of MK1582 (with a *cozEa-gfp* fusion) and MK1584 (with a *cozEb-gfp* fusion) were diluted 1:100 in TSB medium with 100 μg/mL spectinomycin and incubated at 37°C until they reached an OD<sub>600</sub> of approximately 0.4. The cultures were normalized to an OD<sub>600</sub> of 0.4, and subsequently harvested by centrifugation at 4,000 × *g* for 1 minute at 4°C. The pellets were resuspended in 500 μL TSB buffer before being lysed mechanically using the Fast Prep method with ≤106 μm glass beads at 6 m/s. Insoluble material was removed by centrifugation at 20,000 × *g* for 2 minutes. Next, the supernatants were mixed with equal volume 2× SDS loading buffer and heated at 95°C for 5 minutes.

The samples were separated with SDS-PAGE using a polyacrylamide gel, which consisted of a 12% separation gel with a 4% stacking gel layered on top. The subsequent blotting and GFP detection steps were carried out as described in "Immunoblot analysis of lipoteichoic acid in whole cell extracts and supernatants," with the only difference being the selection of antibodies. For detection of GFP-tagged CozE, an anti-GFP primary antibody (Invitrogen) (diluted 1:4,000 in PBST) and an anti-rabbit IgG HRP-conjugated secondary antibody (Promega) (diluted 1:5000 in PBST) were used.

### Split luciferase assay

Pairwise protein-protein interactions were assessed *in vivo* using the split luciferase system developed by Paiva et al. (48) for *C. difficile*, which has previously also been used in *S. aureus* (49). The proteins of interest are fused to either a large (LgBit) or small (SmBit) luciferase subunit, which upon interaction form an active luciferase enzyme. Briefly, overnight cultures of *S. aureus* strains carrying split luciferase plasmids were initially diluted to an OD<sub>600</sub> of 0.05 and cultivated for 90 minutes at 37°C with shaking in the presence of 100 ng/mL anhydrotetracycline and 25 µg/mL chloramphenicol. Luciferase activity was then measured using the Nano-Glo Luciferase Assay System (Promega). The assay reagent was prepared by mixing one volume of the substrate with 50 volumes of buffer, and 20 µL of this reagent was subsequently added to 100 µL of culture. Luminescence (460 nm) and absorbance (OD<sub>600</sub>) were recorded every 15 seconds for a total of five times, in a plate reader (Hidex Sense). The split luciferase data presented in this work are the mean value of four replicate measurements which were normalized to cell density.

### Phylogenetic analysis

CozE homologs were identified with NCBI BLASTp, using the CozEa and CozEb protein sequence of *S. aureus* NCTC8325 as the queries against species within the *Staphylococcaceae* family. In all, 56 CozE homologs belonging to the *Staphylococcaceae*, including CozEa and CozEb found in *S. aureus*, were selected, and subsequently aligned using Clustal Omega (50). Using IQ-TREE (51), the sequence alignment was then used to construct a maximum likelihood phylogenetic tree. Finally, the phylogenetic tree was visualized and annotated with the Interactive Tree Of Life (iTOL) online tool (52).

### Expression and purification of LtaA, CozEa, and CozEb

LtaA and CozE proteins were expressed and purified using the same protocol previously used for the purification of LtaA (35). Briefly, proteins carrying an N-terminal histidine tag were overexpressed in *E. coli* BL21-Gold (DE3) (Stratagene) cells. Cells were grown at 37°C in Terrific Broth medium supplemented with 1% (wt/vol) glucose and induced with 0.2 mM IPTG. Cells were disrupted and membranes were collected by ultracentrifugation. Membranes were solubilized in 50 mM Tris-HCl, pH 8.0; 200 mM NaCl; 20 mM imidazole; 15% (vol/vol) glycerol; 5 mM β-mercaptoethanol; 1% (wt/vol) lauryl maltose neopentyl glycol (LMNG; Anatrace); 1% (wt/vol) N-dodecyl-β-d-maltopyranoside (DDM; Anatrace) for 2 hours at 4°C. After centrifugation, the proteins were purified by affinity chromatography with Ni-NTA superflow affinity column (Qiagen) as previously described (35).

### Formation of proteoliposomes and *in vitro* flipping assay

LtaA and CozE proteins were reconstituted in unilamellar liposomes as described before (35). Briefly, proteoliposomes were prepared by extrusion through polycarbonate filters (400 nm pore size) from a 3:1 (wt/wt) mixture of *E. coli* polar lipids and L-α-phosphatidylcholine (Avanti polar lipids) resuspended in 20 mM Tris-HCl (pH 8.0), 150 mM NaCl, and 2 mM β-mercaptoethanol. After removal of detergent with BioBeads (BioRad), proteoliposomes were centrifugated, washed, and resuspended to a final concentration of 20 mg/mL lipids and flash-frozen in liquid nitrogen and stored at -80°C until further use. Before performing flipping assays, proteoliposomes were thawed, their

resuspension buffer was exchanged to 20 mM MES, pH 6.5; 150 mM NaCl, and the product of the Glc<sub>2</sub>DAG-NBD synthesis was incorporated by performing freeze/thaw cycles. Proteoliposomes and protein-free liposomes were diluted to a concentration of 2 mg/mL lipids followed by extrusion through poly-carbonate filters (400 nm pore size). Proteoliposomes were immediately used for flipping assays (35). Flipping of Glc<sub>2</sub>DAG-NBD was assessed by determining the percentage of NBD-fluorescence that is quenched after the addition of a 5 mM sodium dithionite (Sigma) after 200 seconds of starting fluorescence recording. Before finishing data recording, 0.5% Triton X-100 was added to permeabilize the liposomes, making all Glc<sub>2</sub>DAG-NBD molecules accessible to dithionite reduction. The fluorescence after Triton X-100 addition was used for baseline calculations. Fluorescence was recorded at 20°C using a Jasco Fluorimeter. The excitation and emission wavelengths were 470 and 535 nm, respectively. For analysis, the fluorescence intensity was normalized to F/F<sub>max</sub>. Relative flipping activities were calculated as follows: relative activity =  $100 \times [(F/F_{\max})_i - (F/F_{\max})_{\text{liposomes}}] / [(F/F_{\max})_{\text{wt}} - (F/F_{\max})_{\text{liposomes}}]$ , where *i* corresponds to each respective treatment/mutants, liposomes corresponds to liposomes without protein, wt corresponds to wild-type LtaA, and F/F<sub>max</sub> values correspond to the normalized fluorescence values at the plateau after addition of sodium dithionite. Curves were plotted using GraphPad Prism 8. Time courses of the dithionite-induced fluorescence decay in liposomes were repeated at least three times for each experiment.

## ACKNOWLEDGMENTS

We would like to thank Marita Torrisen Mårli (NMBU) for help with strain construction, Wiep Klaas Smits (Leiden Univ. Medical Center, Netherlands) for providing us with the split luciferase plasmids, Eivind Frøyland Skjennum (NMBU) for help setting up the split luciferase system, and the NMBU Imaging Center for help with transmission electron microscopy.

This work was supported by a grant from the Research Council of Norway (296906, 250976) to M.K., from the Agence Nationale de la Recherche (ANR-19-CE15-0011-01) to C.G., from the Swiss National Science Foundation (310030\_207974 and PP00P3\_198903) to C.P., and from the Swiss National Science Foundation (NCCR AntiResist 51NF40\_180541) to X.L. and J.-W.V.

## AUTHOR AFFILIATIONS

<sup>1</sup>Faculty of Chemistry, Biotechnology and Food Science, Norwegian University of Life Sciences, Ås, Norway

<sup>2</sup>Biozentrum, University of Basel, Basel, Switzerland

<sup>3</sup>Molecular Microbiology and Structural Biochemistry, CNRS UM 5086, Université de Lyon, Lyon, France

<sup>4</sup>Department of Pathogen, Biology, International Cancer Center, Shenzhen University Medical School, Shenzhen, Guangdong, China

<sup>5</sup>Department of Fundamental Microbiology, University of Lausanne, Lausanne, Switzerland

<sup>6</sup>Department of Biochemistry and Molecular Biology, University of Georgia, Athens, Georgia, USA

## AUTHOR ORCIDs

Maria Disen Barbuti  <http://orcid.org/0000-0002-4741-8418>

Jan-Willem Veening  <http://orcid.org/0000-0002-3162-6634>

Daniel Straume  <http://orcid.org/0000-0002-5222-9275>

Morten Kjos  <http://orcid.org/0000-0003-4448-9082>

## FUNDING

Funder	Grant(s)	Author(s)
Norges Forskningsråd (Forskningsrådet)	250976, 296906	Maria Disen Barbuti Ine Storaker Myrbråten Morten Kjos
Agence Nationale de la Recherche (ANR)	ANR-19-CE15-0011-01	Christophe Grangeasse
Schweizerischer Nationalfonds zur Förderung der Wissenschaftlichen Forschung (SNF)	310030_207974, PP00P3_198903	Camilo Perez

## DATA AVAILABILITY

All study data are included in the article and/or supplemental material. All strains and plasmids used in this study are available upon request.

## ADDITIONAL FILES

The following material is available [online](#).

## Supplemental Material

**Supplemental Material (mBio01157-24-S0001.pdf)**. Fig. S1-S14, captions to Movies S1 and S2, and Tables S1-S3.

**Movie S1 (mBio01157-24-s0002.gif)**. The dynamic spatiotemporal localization of GFP-tagged CozEa.

**Movie S2 (mBio01157-24-s0003.gif)**. The dynamic spatiotemporal localization of GFP-tagged CozEb.

## REFERENCES

- Xia G, Kohler T, Peschel A. 2010. The wall teichoic acid and lipoteichoic acid polymers of *Staphylococcus aureus*. *Int J Med Microbiol* 300:148–154. <https://doi.org/10.1016/j.ijmm.2009.10.001>
- Rajagopal M, Walker S. 2017. Envelope structures of Gram-positive bacteria. *Curr Top Microbiol Immunol* 404:1–44. [https://doi.org/10.1007/82\\_2015\\_5021](https://doi.org/10.1007/82_2015_5021)
- Pasquina LW, Santa Maria JP, Walker S. 2013. Teichoic acid biosynthesis as an antibiotic target. *Curr Opin Microbiol* 16:531–537. <https://doi.org/10.1016/j.mib.2013.06.014>
- Oku Y, Kurokawa K, Matsuo M, Yamada S, Lee BL, Sekimizu K. 2009. Pleiotropic roles of polyglycerolphosphate synthase of lipoteichoic acid in growth of *Staphylococcus aureus* cells. *J Bacteriol* 191:141–151. <https://doi.org/10.1128/JB.01221-08>
- Santa Maria JP, Sadaka A, Moussa SH, Brown S, Zhang YJ, Rubin EJ, Gilmore MS, Walker S. 2014. Compound-gene interaction mapping reveals distinct roles for *Staphylococcus aureus* teichoic acids. *Proc Natl Acad Sci U S A* 111:12510–12515. <https://doi.org/10.1073/pnas.1404099111>
- Kiriukhin MY, Debabov DV, Shinabarger DL, Neuhaus FC. 2001. Biosynthesis of the glycolipid anchor in lipoteichoic acid of *Staphylococcus aureus* RN4220: role of Ypfp, the diglycosyldiacylglycerol synthase. *J Bacteriol* 183:3506–3514. <https://doi.org/10.1128/JB.183.11.3506-3514.2001>
- Gründling A, Schneewind O. 2007. Genes required for glycolipid synthesis and lipoteichoic acid anchoring in *Staphylococcus aureus*. *J Bacteriol* 189:2521–2530. <https://doi.org/10.1128/JB.01683-06>
- Zhang B, Liu X, Lambert E, Mas G, Hiller S, Veening JW, Perez C. 2020. Structure of a proton-dependent lipid transporter involved in lipoteichoic acids biosynthesis. *Nat Struct Mol Biol* 27:561–569. <https://doi.org/10.1038/s41594-020-0425-5>
- Gründling A, Schneewind O. 2007. Synthesis of glycerol phosphate lipoteichoic acid in *Staphylococcus aureus*. *Proc Natl Acad Sci U S A* 104:8478–8483. <https://doi.org/10.1073/pnas.0701821104>
- Kho K, Meredith TC. 2018. Salt-induced stress stimulates a lipoteichoic acid-specific three-component glycosylation system in *Staphylococcus aureus*. *J Bacteriol* 200:e00017-18. <https://doi.org/10.1128/JB.00017-18>
- Rismondo J, Gillis A, Gründling A. 2021. Modifications of cell wall polymers in Gram-positive bacteria by multi-component transmembrane glycosylation systems. *Curr Opin Microbiol* 60:24–33. <https://doi.org/10.1016/j.mib.2021.01.007>
- Corrigan RM, Abbott JC, Burhenne H, Kaever V, Gründling A. 2011. c-di-AMP is a new second messenger in *Staphylococcus aureus* with a role in controlling cell size and envelope stress. *PLoS Pathog* 7:e1002217. <https://doi.org/10.1371/journal.ppat.1002217>
- Bæk KT, Bowman L, Millership C, Dupont Søgaard M, Kaever V, Siljamäki P, Savijoki K, Varmanen P, Nyman TA, Gründling A, Frees D. 2016. The cell wall polymer lipoteichoic acid becomes nonessential in *Staphylococcus aureus* cells lacking the ClpX chaperone. *mBio* 7:e01228-16. <https://doi.org/10.1128/mBio.01228-16>
- Hesser AR, Matano LM, Vickery CR, Wood BM, Santiago AG, Morris HG, Do T, Losick R, Walker S. 2020. The length of lipoteichoic acid polymers controls *Staphylococcus aureus* cell size and envelope integrity. *J Bacteriol* 202:e00149-20. <https://doi.org/10.1128/JB.00149-20>
- Reichmann NT, Gründling A. 2011. Location, synthesis and function of glycolipids and polyglycerolphosphate lipoteichoic acid in Gram-positive bacteria of the phylum *Firmicutes*. *FEMS Microbiol Lett* 319:97–105. <https://doi.org/10.1111/j.1574-6968.2011.02260.x>
- Hesser AR, Schaefer K, Lee W, Walker S. 2020. Lipoteichoic acid polymer length is determined by competition between free starter units. *Proc Natl Acad Sci U S A* 117:29669–29676. <https://doi.org/10.1073/pnas.2008929117>

17. Burtchett TA, Shook JC, Hesse LE, Delekta PC, Brzozowski RS, Nouri A, Calas AJ, Spanoudis CM, Eswara PJ, Hammer ND. 2023. Crucial role for lipoteichoic acid assembly in the metabolic versatility and antibiotic resistance of *Staphylococcus aureus*. *Infect Immun* 91:e0055022. <https://doi.org/10.1128/iai.00550-22>
18. Schneewind O, Missiakas D. 2019. Lipoteichoic acid synthesis and function in Gram-positive bacteria, p 163–180. In Geiger O (ed), *Biogenesis of fatty acids, lipids and membranes*. Springer International Publishing, Cham. [https://doi.org/10.1007/978-3-319-50430-8\\_17](https://doi.org/10.1007/978-3-319-50430-8_17).
19. Reichmann NT, Piçarra Cassona C, Monteiro JM, Bottomley AL, Corrigan RM, Foster SJ, Pinho MG, Gründling A. 2014. Differential localization of LTA synthesis proteins and their interaction with the cell division machinery in *Staphylococcus aureus*. *Mol Microbiol* 92:273–286. <https://doi.org/10.1111/mmi.12551>
20. Barbuti MD, Myrbråten IS, Morales Angeles D, Kjos M. 2023. The cell cycle of *Staphylococcus aureus*: an updated review. *Microbiologyopen* 12:e1338. <https://doi.org/10.1002/mbo3.1338>
21. Fenton AK, El Mortaji L, Lau DTC, Rudner DZ, Bernhardt TG. 2016. CozE is a member of the MreCD complex that directs cell elongation in *Streptococcus pneumoniae*. *Nat Microbiol* 2:16237. <https://doi.org/10.1038/nmicrobiol.2016.237>
22. Straume D, Stamsås GA, Berg KH, Salehian Z, Håvarstein LS. 2017. Identification of pneumococcal proteins that are functionally linked to penicillin-binding protein 2b (PBP2b). *Mol Microbiol* 103:99–116. <https://doi.org/10.1111/mmi.13543>
23. Ducret A, Grangeasse C. 2017. Bacterial physiology: wrapping the cell in a CozE shell. *Nat Microbiol* 2:16262. <https://doi.org/10.1038/nmicrobiol.2016.262>
24. Jana B, Liu X, Dénéreaz J, Park H, Leshchiner D, Liu B, Gallay C, Veening J-W, van Opijnen T. 2023. CRISPRi-TnSeq: a genome-wide high-throughput tool for bacterial essential-nonessential genetic interaction mapping. *bioRxiv*. <https://doi.org/10.1101/2023.05.31.543074>
25. Stamsås GA, Restelli M, Ducret A, Fretton C, Garcia PS, Håvarstein LS, Straume D, Grangeasse C, Kjos M. 2020. A CozE homolog contributes to cell size homeostasis of *Streptococcus pneumoniae*. *mBio* 11:e02461-20. <https://doi.org/10.1128/mBio.02461-20>
26. Stamsås GA, Myrbråten IS, Straume D, Salehian Z, Veening J-W, Håvarstein LS, Kjos M. 2018. CozEa and CozEb play overlapping and essential roles in controlling cell division in *Staphylococcus aureus*. *Mol Microbiol* 109:615–632. <https://doi.org/10.1111/mmi.13999>
27. Fey PD, Endres JL, Yajjala VK, Widhelm TJ, Boissy RJ, Bose JL, Bayles KW. 2013. A genetic resource for rapid and comprehensive phenotype screening of nonessential *Staphylococcus aureus* genes. *mBio* 4:e00537-12. <https://doi.org/10.1128/mBio.00537-12>
28. Monteiro JM, Fernandes PB, Vaz F, Pereira AR, Tavares AC, Ferreira MT, Pereira PM, Veiga H, Kuru E, VanNieuwenhze MS, Brun YV, Filipe SR, Pinho MG. 2015. Cell shape dynamics during the staphylococcal cell cycle. *Nat Commun* 6:8055. <https://doi.org/10.1038/ncomms9055>
29. Arnaud M, Chastanet A, Débarbouillé M. 2004. New vector for efficient allelic replacement in naturally nontransformable, low-GC-content, Gram-positive bacteria. *Appl Environ Microbiol* 70:6887–6891. <https://doi.org/10.1128/AEM.70.11.6887-6891.2004>
30. Liu X, de Bakker V, Heggenhougen MV, Mårli MT, Frøynes AH, Salehian Z, Porcellato D, Angeles DM, Veening J-W, Kjos M. 2023. Genome-wide CRISPRi screens reveal the essentialome and determinants for susceptibility to dalbavancin in *Staphylococcus aureus*. *bioRxiv*. <https://doi.org/10.1101/2023.08.30.555613>
31. Kuru E, Tekkam S, Hall E, Brun YV, Van Nieuwenhze MS. 2015. Synthesis of fluorescent D-amino acids and their use for probing peptidoglycan synthesis and bacterial growth *in situ*. *Nat Protoc* 10:33–52. <https://doi.org/10.1038/nprot.2014.197>
32. Coe KA, Lee W, Stone MC, Komazin-Meredith G, Meredith TC, Grad YH, Walker S. 2019. Multi-strain Tn-Seq reveals common daptomycin resistance determinants in *Staphylococcus aureus*. *PLoS Pathog* 15:e1007862. <https://doi.org/10.1371/journal.ppat.1007862>
33. Mikkelsen K, Sirisarn W, Alharbi O, Alharbi M, Liu H, Nøhr-Meldgaard K, Mayer K, Vestergaard M, Gallagher LA, Derrick JP, McBain AJ, Biboy J, Vollmer W, O'Gara JP, Grunert T, Ingmer H, Xia G. 2021. The novel membrane-associated auxiliary factors AuxA and AuxB modulate  $\beta$ -lactam resistance in MRSA by stabilizing lipoteichoic acids. *Int J Antimicrob Agents* 57:106283. <https://doi.org/10.1016/j.ijantimicag.2021.106283>
34. Peschel A, Vuong C, Otto M, Götz F. 2000. The D-alanine residues of *Staphylococcus aureus* teichoic acids alter the susceptibility to vancomycin and the activity of autolytic enzymes. *Antimicrob Agents Chemother* 44:2845–2847. <https://doi.org/10.1128/AAC.44.10.2845-2847.2000>
35. Lambert E, Mehdipour AR, Schmidt A, Hummer G, Perez C. 2022. Evidence for a trap-and-flip mechanism in a proton-dependent lipid transporter. *Nat Commun* 13:1022. <https://doi.org/10.1038/s41467-022-28361-1>
36. Leshchiner D, Rosconi F, Sundaresh B, Rudmann E, Ramirez LMN, Nishimoto AT, Wood SJ, Jana B, Buján N, Li K, Gao J, Frank M, Reeve SM, Lee RE, Rock CO, Rosch JW, van Opijnen T. 2022. A genome-wide atlas of antibiotic susceptibility targets and pathways to tolerance. *Nat Commun* 13:3165. <https://doi.org/10.1038/s41467-022-30967-4>
37. Guyet A, Alofi A, Daniel RA. 2023. Insights into the roles of lipoteichoic acids and MprF in *Bacillus subtilis*. *mBio* 14:e0266722. <https://doi.org/10.1128/mbio.02667-22>
38. Steele VR, Bottomley AL, Garcia-Lara J, Kasturiarachchi J, Foster SJ. 2011. Multiple essential roles for EzrA in cell division of *Staphylococcus aureus*. *Mol Microbiol* 80:542–555. <https://doi.org/10.1111/j.1365-2958.2011.07591.x>
39. Liu X, Van Maele L, Matarazzo L, Souldard D, Alves Duarte da Silva V, de Bakker V, Dénéreaz J, Bock FP, Taschner M, Gruber S, Nizet V, Sirard J-C, Veening J-W. 2023. A conserved antigen induces respiratory Th17-mediated serotype-independent protection against pneumococcal superinfection. *bioRxiv*. <https://doi.org/10.1101/2023.07.07.548156>
40. Heß N, Waldow F, Kohler TP, Rohde M, Kreikemeyer B, Gómez-Mejía A, Hain T, Schwudke D, Vollmer W, Hammerschmidt S, Gisch N. 2017. Lipoteichoic acid deficiency permits normal growth but impairs virulence of *Streptococcus pneumoniae*. *Nat Commun* 8:2093. <https://doi.org/10.1038/s41467-017-01720-z>
41. Müller A, Wenzel M, Strahl H, Grein F, Saaki TNV, Kohl B, Siersma T, Bandow JE, Sahl HG, Schneider T, Hamoen LW. 2016. Daptomycin inhibits cell envelope synthesis by interfering with fluid membrane microdomains. *Proc Natl Acad Sci U S A* 113:E7077–E7086. <https://doi.org/10.1073/pnas.1611173113>
42. Grein F, Müller A, Scherer KM, Liu X, Ludwig KC, Klöckner A, Strach M, Sahl HG, Kubitscheck U, Schneider T. 2020. Ca<sup>2+</sup>-daptomycin targets cell wall biosynthesis by forming a tripartite complex with undecaprenyl-coupled intermediates and membrane lipids. *Nat Commun* 11:1455. <https://doi.org/10.1038/s41467-020-15257-1>
43. Wang Y, Kinoshita T. 2023. The role of lipid scramblases in regulating lipid distributions at cellular membranes. *Biochem Soc Trans* 51:1857–1869. <https://doi.org/10.1042/BST20221455>
44. Löfblom J, Kronqvist N, Uhlén M, Ståhl S, Wernérus H. 2007. Optimization of electroporation-mediated transformation: *Staphylococcus carnosus* as model organism. *J Appl Microbiol* 102:736–747. <https://doi.org/10.1111/j.1365-2672.2006.03127.x>
45. Charpentier E, Anton AI, Barry P, Alfonso B, Fang Y, Novick RP. 2004. Novel cassette-based shuttle vector system for Gram-positive bacteria. *Appl Environ Microbiol* 70:6076–6085. <https://doi.org/10.1128/AEM.70.10.6076-6085.2004>
46. Helle L, Kull M, Mayer S, Marincola G, Zelder ME, Goerke C, Wolz C, Bertram R. 2011. Vectors for improved Tet repressor-dependent gradual gene induction or silencing in *Staphylococcus aureus*. *Microbiology (Reading)* 157:3314–3323. <https://doi.org/10.1099/mic.0.052548-0>
47. Ducret A, Qardokus EM, Brun YV. 2016. MicrobeJ, a tool for high throughput bacterial cell detection and quantitative analysis. *Nat Microbiol* 1:16077. <https://doi.org/10.1038/nmicrobiol.2016.77>
48. Oliveira Paiva AM, Friggen AH, Qin L, Douwes R, Dame RT, Smits WK. 2019. The bacterial chromatin protein HupA can remodel DNA and associates with the nucleoid in *Clostridium difficile*. *J Mol Biol* 431:653–672. <https://doi.org/10.1016/j.jmb.2019.01.001>
49. Wood A, Irving SE, Bennisson DJ, Corrigan RM. 2019. The (p)ppGpp-binding GTPase Era promotes rRNA processing and cold adaptation in *Staphylococcus aureus*. *PLoS Genet* 15:e1008346. <https://doi.org/10.1371/journal.pgen.1008346>
50. Sievers F, Wilm A, Dineen D, Gibson TJ, Karplus K, Li W, Lopez R, McWilliam H, Remmert M, Söding J, Thompson JD, Higgins DG. 2011.

- Fast, scalable generation of high-quality protein multiple sequence alignments using Clustal Omega. *Mol Syst Biol* 7:539. <https://doi.org/10.1038/msb.2011.75>
51. Nguyen L-T, Schmidt HA, von Haeseler A, Minh BQ. 2015. IQ-TREE: a fast and effective stochastic algorithm for estimating maximum-likelihood phylogenies. *Mol Biol Evol* 32:268–274. <https://doi.org/10.1093/molbev/msu300>
52. Letunic I, Bork P. 2021. Interactive tree of life (iTOL) v5: an online tool for phylogenetic tree display and annotation. *Nucleic Acids Res* 49:W293–W296. <https://doi.org/10.1093/nar/gkab301>